Controlled Coherent Excitations in a Single Cadmium Ion with an Ultrafast Laser

by

Rudolph Nicolas Kohn Jr.

A senior honors thesis submitted to

the Department of Physics of

the University of Michigan

College of Literature, Science and the Arts

in partial fullfilment of the requirements

for the degree of

Honors B.S. in Physics

2006

and for consideration for the Williams Prize.

This thesis entitled:
Controlled Coherent Excitations in a Single Cadmium Ion with an Ultrafast Laser
written by R. N. Kohn Jr.
has been approved for submittal by

_____
Prof. Christopher Monroe

Date _____

_____
Rudolph N. Kohn Jr.

Date _____

The final copy of this thesis has been examined by the research advisor and has been found suitable for completion of the requirements.

Abstract

Coherent transitions between quantum states form the basis for quantum computation algorithms. We demonstrate the coherent drive of a qubit state stored in hyperfine states of a single trapped cadmium ion to an electronically excited state with a laser pulse short compared to the lifetime of the excited state. The transitions are demonstrated by observation of Rabi flopping with pulses of varying energy, and coherence is demonstrated by the disappearance and reappearance of contrast upon application of ultrafast pulses in a Ramsey interferometer. This ultrafast coupling is vital in a scheme for generation of entangled networks of remote ion qubits via photon interference, and generates a specific momentum kick of $2\hbar k$ which is a fundamental requirement for the implementation of ultrafast quantum gates.

Acknowledgements

First, I would like to thank all the members of Prof. Chris Monroe's group here; without them none of this would have happened, and I might be a chemist right now... Special thanks go to Prof. Boris Blinov, Martin Madsen, Dr. Peter Maunz, David Moehring, and Prof. Chris Monroe for all of the time they've spent helping me find a place in the ultrafast group. I also want to thank Martin, Peter, and Dave for working on this experiment with me, and for providing advice, help, and answers about it whenever I asked. I want to thank Peter, Prof. Monroe, and Martin for their help with revisions and proofreading, as well. Prof. Monroe also was instrumental in the work on this experiment, lending us his keen insights into the workings of the experiment. I also must thank Prof. Monroe for the opportunity to work on this experiment and to work with this group.

Contents

Chapter

Figures

Figure

Chapter 1

Introduction

1.1 Ion Trapping and Quantum Computing

The first ion traps were built by Wolfgang Paul in the 1950's [1]. Since then, ion traps have found a wealth of applications in a variety of fields. For instance, the g-factor of the electron was measured to two parts in 10^{12} in a Penning trap [2]. Ion traps have been used to study the dynamics of entangled states and the generation of entanglement and Schrödinger's cat states[3, 4, 5], to measure excited state lifetimes [6], and even to study biological compounds [7]. Though ion traps have been put to excellent use in many fields, they have been especially useful in the field of quantum computing [8]. In 1994, Peter Shor invented an algorithm which uses quantum bits, or qubits, to factor large numbers with exponentially fewer operations than known classical algorithms [9]. Peter Shor's factoring algorithm uses the fact that qubits can exist in superpositions of both states, unlike classical bits, which can only exist in one of two states at any time. In a quantum computer, operations can affect all of the states superposed in the system. An additional use of quantum computing was devised by Lov Grover: a quantum computer is capable of searching a large unsorted database significantly faster than current classical algorithms [10]. These algorithms have numerous applications, making quantum computation incredibly useful.

The basic requirements for the construction of a quantum computer are laid out by DiVincenzo [11]. There are five basic requirements:

(1) The system must be scalable and have well-defined qubits.

(2) One must be able to initialize the qubit state(s) to a known value.

(3) Coherence times of the qubit must be long compared to the relevant operation times; at a bare minimum, the qubit state must last much longer than the time it takes to perform an operation on the qubit, but storage of information requires essentially indefinite coherence.

(4) A set of quantum gates which can universally manipulate the system must exist and be implementable.

(5) The qubit state must be measurable.

Trapped cadmium ion systems satisfy all of these requirements.

In trapped cadmium ion systems, the qubit is usually represented by a pair of hyperfine states in the ground electronic state ($5s\ ^2S_{1/2}$). The two states have separation of about 14.5 GHz, much larger than the linewidth of the upper state. Thus, the two states are well-defined. Entanglement in trapped ion systems, including cadmium, has been thoroughly demonstrated [3, 4]. Ion trap geometries with multiple trapping regions are commonly used and easily constructed, and addition of sites for storage of additional ions presents negligible overhead [12]. In addition, schemes which permit movement of ions from one trapping region to another have been demonstrated [13]. Thus, cadmium trapped ion systems are scalable as well, satisfying the first requirement.

The second and fifth requirements are dealt with by the procedure of optical pumping. In cadmium ion systems, the state can be initialized by optically pumping the ion population to one of the two qubit states, and the measurement is performed by optically pumping a cycling transition with a continuous-wave laser. Of the two qubit states, one is excited by the laser and scatters enormous numbers of photons. The other is detuned due to hyperfine splitting by many linewidths, and is not excited. The number of photons we collect in a given time period

is strongly correlated to the qubit state, making measurement of the qubit state with extremely high accuracy possible.

In order to satisfy the third requirement, we commonly use the first-order Zeeman insensitive hyperfine states to represent the qubit. The lifetime of the upper state is on the order of thousands of years, meaning that direct decay from one qubit state to another is extremely unlikely on the time scale of nearly any experiment. In addition, the use of first-order Zeeman insensitive states means that phase decoherence caused by magnetic field noise can be minimized quite easily in the low-magnetic-field regime. In addition, gate times in trapped cadmium ion systems are on the order of microseconds, far less than the decoherence time.

In the field of quantum computing, there are two gates which form a "universal" set: the arbitrary qubit rotation and the controlled-not gate. Single qubit rotations affect the state of one (and only one) qubit, imparting a change of state or a relative phase. Controlled-NOT (CNOT) gates couple the states of two qubits. By convention, the first qubit in a CNOT gate is designated the control qubit. The state of the second qubit is inverted depending on the state of the control. The CNOT gate has the truth table:

$$|00\rangle \rightarrow |00\rangle$$

$$|01\rangle \rightarrow |01\rangle$$

$$|10\rangle \rightarrow |11\rangle$$

$$|11\rangle \rightarrow |10\rangle$$

Both gates have been implemented in trapped ion systems, including cadmium systems, with high fidelity [8, 14, 15].

The theory and implementation of the CNOT gate in trapped ion systems has been thoroughly studied. Many of the proposals for the implementation of the CNOT gate in trapped ion systems relies on coupling the collective motion of two trapped ions with their qubit states. However, in order to couple motional states in a coherent way, the ions must be brought to a

known motional state. The difficulty comes from the fact that the motional state occupation depends on the thermal state of the ions. Therefore, the ions must be cooled to ensure that the system is in a coherent state. The proposal by Cirac and Zoller requires cooling to the ground state, and the proposal by Mølmer and Sørenson requires cooling only to within the Lamb-Dicke limit [8, 16]. Although such cooling is difficult experimentally, gates using this method have been realized experimentally in trapped ion systems [14, 15].

Recent theoretical progress in trapped-ion manipulation has shown that implementation of quantum gates without stringent requirements on the motional state of the ion is possible [17, 18, 19, 20, 21, 22]. The theory suggests that implementation of quantum gates without cooling to the ground state is possible with the use of ultrafast laser pulses. The coherent manipulation of state populations with ultrafast laser pulses is thus a fundamental requirement of these gates.

The demonstration of such ultrafast coupling was the purpose of the experiment described in this thesis. We first demonstrate controlled excitation by showing that ultrafast laser pulses are capable of controlled excitation of ions in a Rabi experiment. We then demonstrate the coherence of these manipulations by placing the controlled excitations in a Ramsey interferometer. The disappearance and revival of contrast in the Ramsey fringes demonstrates that the pulsed laser excitation is coherent. This coherent excitation and de-excitation, and the resulting momentum kick on the ion are fundamental to the implementation of ultrafast quantum gates.

Chapter 2

Theory

In this chapter, the discussion covers briefly some theoretical aspects of this experiment. First covered are the basics of ion traps, followed by treatment of the electronic structure of our chosen system, cadmium ions. Next, the theoretical aspects of the preparation of the ion state in several configurations is discussed. Subsequently, the phenomenon of laser excitation of two-level systems is examined, followed by a brief coverage of Ramsey interferometry.

2.1 Ion Traps

Ion traps work on the principle of a pseudopotential. The goal is to generate a field which confines an ion in all directions. A static field which meets that requirement points inward in all directions. However, Maxwell's law in a vacuum requires that electric fields in a vacuum have zero divergence, and a field pointing inward in all directions has negative divergence. Therefore, the field lines must somewhere escape from the center of any static field. Thus, it is impossible to use a static field to trap a charged particle. Instead, by rapidly varying the field in two axes, a pseudopotential is created which can trap the ion [23]. Linear rf quadrupole traps like the ones used in our experiment (see Fig. 2.1) have six electrodes. An oscillating voltage is applied to two electrodes, and two more act as radiofrequency grounds. To the remaining two electrodes are applied static voltages. The four rf electrodes, two at high voltage and two grounded, dynamically trap the ion in two dimensions. The latter two act as endcaps, statically trapping the ion in the remaining dimension.

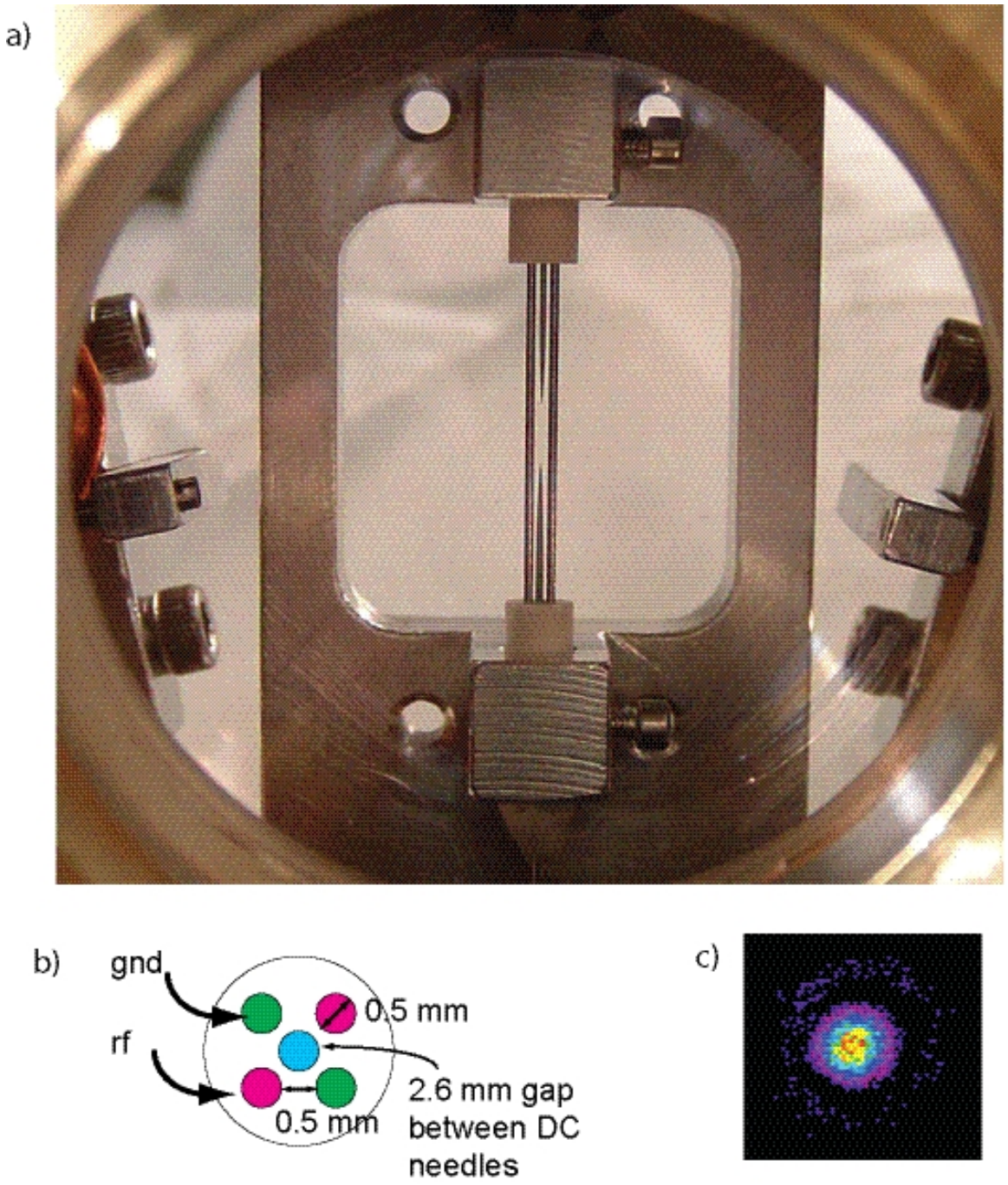

Figure 2.1: (a) A photograph of the trap used in this experiment. The trap consists of four tungsten rods and two needles arranged in order to be used as a linear rf Paul trap. (b) A cross-sectional view of the trap. High-voltage rf is applied to two rods, the other two are held at rf ground, dynamically trapping ions in directions transverse to the rods. The needles serve as the DC electrodes, statically trapping the ions along the axial direction. (c) CCD data showing an illuminated single ion. The color of the picture is determined by the number of photons collected by the CCD.

The dynamics of the system are described by the Mathieu equations, which have a solution that is simple enough to understand qualitatively–the ion exhibits two types of motion, commonly called secular motion and micromotion, which are sinusoidal in nature and occur simultaneously. Secular motion occurs at the "trap frequency," which depends on the mass and charge of the trapped particle, the voltages applied, the rf drive frequency, and the dimension of the trap, but is generally much less than the rf drive frequency. Typical trap frequencies for ion traps are on the order of 1 MHz. Micromotion has the same frequency as the rf drive, and its magnitude is proportional to the distance of the ion from the center of the trap. Micromotion is commonly nulled by applying static voltages to the ground electrodes in order to eliminate stray electric fields and set the ion in the center of the trap [24].

2.2 Cadmium

2.2.1 Electronic Structure

Cd^+ has one valence electron, giving it a general structure analogous to that of hydrogen. Instead of looking in the $\mid l, m\rangle$ basis, however, we look in the hyperfine spin, or $|F, m_F\rangle$, basis. Isotopes of Cd with even atomic mass (106,108,110,112,114,116) have no nuclear spin, and therefore no hyperfine structure, so their spectra are especially simple. The "ground" energy level of even isotopes of Cd+ is a 5s $^2S_{1/2}$ state, with a 5p $^2P_{1/2}$ state 226.5 nm above and a 5p $^2P_{3/2}$ state 214.5 above. The odd isotopes (111,113) have similar spectra, with added hyperfine structure and Zeeman splitting.

Pictured in Fig. 2.2 is a diagram of the energy levels of $^{111}Cd^+$ in the $\mid F, m_F\rangle$ basis, where F is the hyperfine spin quantum number, $\vec{F} = \vec{I} + \vec{J}$, with $\vec{I}$ the nuclear spin and $\vec{J}$ the total angular momentum of the electron. In this basis, single photon transitions obey the selection rules $\Delta F = \pm 1$ or 0 and $\Delta m_F = 0$ or ± 1. Additionally forbidden are transitions where $\Delta F = 0$ when $m_F = 0$. The change in m_F is determined by the polarization of the photon, where light linearly polarized parallel to the quantization axis (the axis of the magnetic

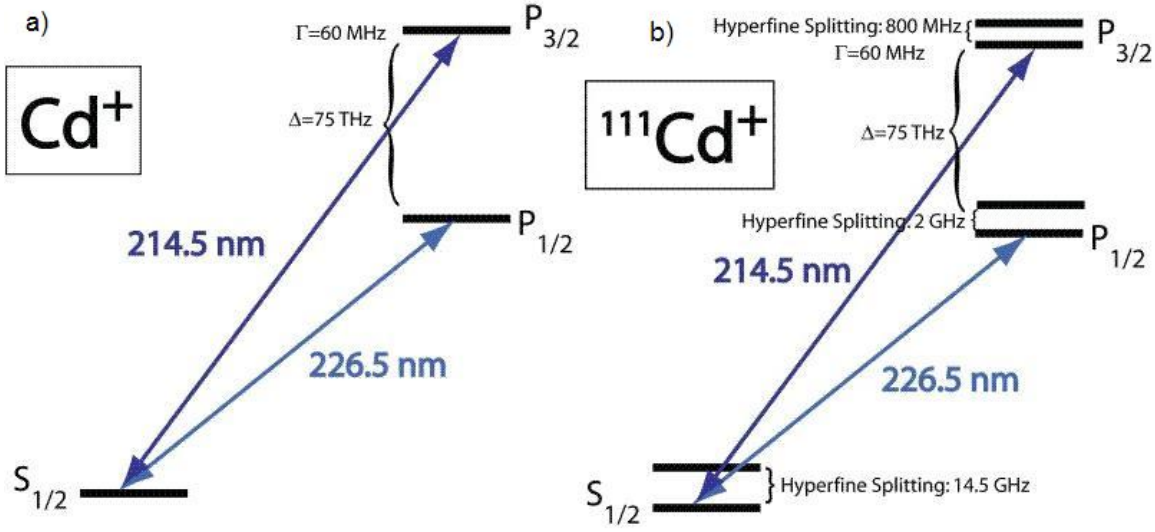

Figure 2.2: Diagrams of relevant energy levels for cadmium ions. (a) Fine structure for even isotopes of Cd^+. (b) Fine structure and hyperfine structure for $^{111}Cd^+$.

field experienced by the ion) is π light, and excites transitions with $\Delta m_F = 0$. Right-circularly polarized light with respect to the quantization axis is termed σ^+ light, and excites transitions with $\Delta m_F = 1$. Conversely, left-circularly polarized light is σ^- light, and excites transitions with $\Delta m_F = -1$.

An obvious difference between the spectra of hydrogen and cadmium is the inverted structure of the hyperfine splitting. This is due to cadmium's negative nuclear g-factor. Hyperfine splitting is caused by interaction between the magnetic field caused by the nucleus and the electron. In hydrogen, the nucleus consists of a single proton with a positive g-factor. The energy splitting between the hyperfine levels in hydrogen is proportional to the dipole moment of the proton, which has the same sign as the angular momentum of the electron. In cadmium, the sign of the dipole moment is reversed (due to the negative g-factor), reversing the direction of the splitting. The experimental result is that the hyperfine levels of the odd isotopes of $^{111}Cd^+$are split by 14.5 GHz, with the triplet having lower energy than the singlet.

The structures for different isotopes differ slightly. While the overall structure remains essentially the same, the frequency splittings between levels change slightly, making slight adjustments of the light frequency necessary when using different isotopes. The best-characterized and most often used shifts are of the $S_{1/2}$ to $P_{3/2}$ transition, which changes over a range of about 6 GHz for all isotopes. The shortest wavelength for this transition occurs for $^{111}Cd^+$, when our laser is tuned to 858.0261 nm, and the longest occurs for $^{116}Cd^+$, at 858.0292 nm. The given wavelengths are shifted by about 200 MHz by acousto-optic modulators in the beam and frequency-quadrupled in nonlinear crystals, resulting in light at the correct wavelength being applied to the ion.

2.2.2 Photoionization

The form of the trap pseudopotential can be approximated by a harmonic well. The trap has a depth of at least several hundred kelvins, far above room temperature. If we created our ions far from the center of the trap, their energies would be increased by amounts corresponding

to the pseudopotential at their position when created (thousands of kelvins). Therefore, if we wanted to create ions far from the center of the trap, we would need to cool them by a huge amount in order to trap them. Moreover, such cooling is not realizable experimentally. On the other hand, if we generate ions at the center of the trap, they see a potential barrier of several hundred kelvins, and cannot escape.

In order to create ions in the center of the trap, we need neutral cadmium in the trapping region. Fortunately, the vapor pressure of cadmium at room temperature is large enough that if cadmium metal is present in the vacuum chamber near the trap, there will be cadmium vapor present in the trapping area. The sources of cadmium are ovens filled with the metal and pointed at the trap. These ovens can be supplied with a current in order to create a hot cadmium vapor in the trapping area, but in practice the firing of these ovens is rarely, if ever, necessary. The room temperature vapor pressure of cadmium is sufficient.

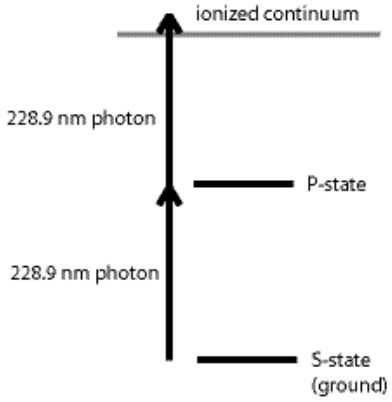

Figure 2.3: Diagram of relevant energy levels for ionization of neutral cadmium. A mode-locked, frequency-quadrupled femtosecond laser is tuned to the transition between neutral S and P states at about 228.9 nm and directed onto the trapping region. Neutral cadmium vapor present in this region are excited by the intense light pulses, and are ionized in a two-photon process.

Cadmium metal in the trapping region is ionized by a two-photon process (see Fig. 2.3) in which an electron in cadmium's ground state is excited to a P state, which happens to be close enough to the ionized state that a second photon can ionize the cadmium. The light is provided by a mode-locked femtosecond laser tuned to approximately 915 nm. The light of these pulses is frequency-quadrupled in order to excite the S-to-P transition. The pulses come

every 12 nanoseconds, and are focused down to approximately 10 microns. Cadmium atoms passing through the beam are ionized by the intense laser pulses, resulting in trapped cadmium ions. After the ions are generated in the trap, they are cooled by the continuous-wave Doppler cooling laser which is generally left on while loading. However, the ions loaded this way remain in the trap whether we cool them immediately or not, as we have observed ions in the trap after loading without the Doppler beam on.

2.3 Doppler Cooling, State Preparation and Detection

Doppler cooling is a method to reduce the energy of a system by exposing it to radiation whose frequency is of order one linewidth red of some closed transition. If the system is moving in the same direction as the light, it sees the light as even further red-detuned due to Doppler shift, and has smaller probability of absorbing a photon. Conversely, if it moves against the light, it sees the light as even closer to resonance, and has a higher absorption probability. Since the resulting photon scatter has random direction, the net effect is a decrease in overall velocity of the system and a corresponding decrease in temperature [25].

The fact that doppler cooling relies on Doppler shifted photons exciting a transition with finite linewidth means that there is a fundamental limit to the energy levels achievable with this method. The minimum average kinetic energy achievable by Doppler cooling is $\frac{1}{4}\hbar\gamma$ [25], where γ is the linewidth. For our system, the linewidth is 60 MHz, and the trap is well-approximated by a harmonic well with frequency $\omega = 0.9$ MHz, leading to a minimum average occupation level of $\approx$40. For our three-dimensional trap, the minimum average energy occupation level achievable in the i-axis of the trap is $n_D \approx \gamma/2\omega_i$ [26].

The light we use to cool the ion is tuned about one linewidth red of the $S_{1/2}$ $F = 1$ to $P_{3/2}$ $F = 2$ transition at approximately 214.5 nm, and it is σ^+ polarized. It is tuned closely enough that with a few hundred microwatts of laser power focused on the ion, we observe tens of thousands of scattered photons per second if the ion is in the $F = 1$ manifold, resulting in cooling to the Doppler limit after a few hundred microseconds.

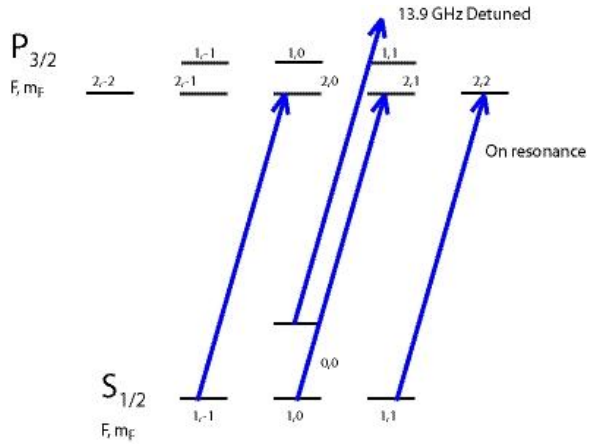

Figure 2.4: Diagram of relevant energy levels for Doppler cooling of $^{111}Cd^{+}$. Note that the $\mid 0,0\rangle$ state is detuned by ~ 14 GHz. In order to cool the dark state, we add 14 GHz sidebands to the laser so that the $\mid 0,0\rangle$ level couples to the $\mid 1,1\rangle$ level in the P manifold. When detecting, we do not add sidebands, and only the states in the $F = 1$ manifold scatter photons. All three of the states are equally bright.

The light is tuned so that it excites the $S_{1/2}$ $F = 1$ manifold to the $P_{3/2}$ $F = 2$ manifold, but examination of the energy level structure (Fig. 2.4) shows that, if the ion is in the $F = 0$ manifold, the light is 13.9 GHz detuned from the transition from $S_{1/2}$ $F = 0$ to $P_{3/2}$ $F = 1$. Since the linewidth of that transition is $\approx$ 60 MHz, the laser is too far away to excite the transition. In order to cool the ion in any state, it is necessary to use a microwave-driven electro-optic modulator (EOM) to add appropriate sidebands to the laser, in order to excite the aforementioned transition. Thus, when we cool the ion, we turn on the EOM in order to cool all possible ion states.

When we want to detect the ion state, we apply the cooling beam without turning on the EOM. In this way, if the ion is in the $F = 1$ manifold, it scatters tens of thousands of photons per second. We call this state the "bright" state. All three states in the $F = 1$ manifold are equally bright under these conditions [27]. In the $F = 0$ manifold, without the EOM, the ion scatters almost no light. Therefore, we call the $F = 0$ manifold the "dark" state 2.5.

For a given detection time and laser power, the two states have distinctive brightness histograms of counts per experiment, shown in Fig. 2.5. When we detect the ion in an unknown state, we measure photon counts per experiment for a large number ($\approx$ 1000) of experiments. The resulting histograms can be fit to a linear combination of the two known state histograms, resulting in state detection with $\sim$ 99% accuracy.

State initialization requires us to pump the ion into the dark state. In order to do that, we turn off the EOM and apply π-polarized light. Population in the bright state is pumped to the dark state after a few tens of microseconds. Population in the dark state is too far off-resonant to be excited by the applied laser. In this way, we prepare the ion in the $\mid 0, 0\rangle$ state. After the state is prepared, we perform an experiment, measure the state of the ion, and once again cool the ion in less than a millisecond. The experiment is computer-controlled, repeating hundreds of times per second.

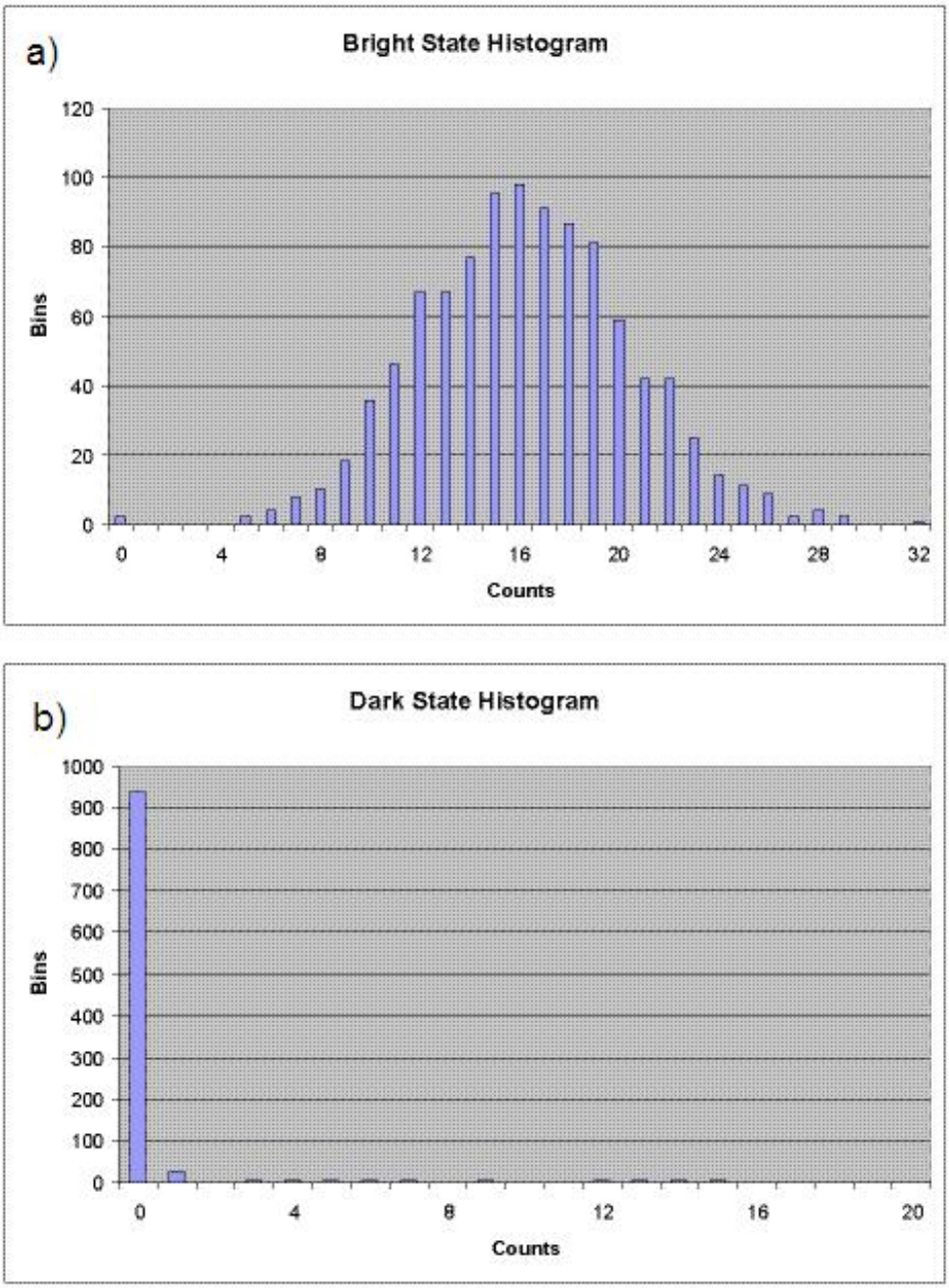

Figure 2.5: Examples of histograms for the bright (a) and dark (b) states. Note that almost all of the experiments in the dark state scatter zero photons, and almost none of the experiments in the bright state scatter less than five. The extremely small overlap between these two histograms means any measured histogram can be fit to a linear combination of these two with very little ambiguity. The result of such a fit is a probability to be found in the bright or dark state.

2.4 Rabi Oscillations

An extremely important phenomenon, is the excitation of a two-level system by nearly resonant electromagnetic waves. The results here are useful almost anytime light with a well-defined frequency is applied to a system with electromagnetic transitions. The key to the solution is the rotating wave approximation, which simplifies the resulting differential equations so that they can be solved exactly [28].

For simplicity, we consider a two-level system. We note that complex systems can be approximated as a two-level system when coupling only occurs between two levels at a time, as is the case in this experiment. We assume that there are two eigenstates of the unperturbed Hamiltonian, H^0, which we designate $|\psi_a\rangle$ and $|\psi_b\rangle$. These two eigenstates have energy separation $\hbar\omega_0$ (See Fig. 2.6).

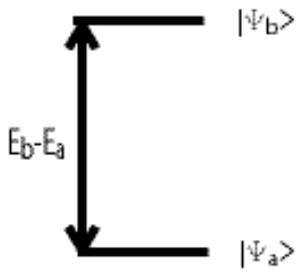

Figure 2.6: A diagram of the energy levels of a two-level system, separated by a known, non-zero energy.

We then turn on an interaction Hamiltonian, $H'(t)$. We know that the system can be completely expressed in general by

$$\psi(t) = c_a(t)e^{-iE_at/\hbar}|\psi_a\rangle + c_b(t)e^{-iE_bt/\hbar}|\psi_b\rangle$$

where E_a and E_b are the eigenenergies of states a and b, respectively, and $c_a(t)$ and $c_b(t)$ are functions of time which are represented by a complex number. From there, we apply the time-dependent Schrödinger equation, $H\psi = i\hbar\frac{\partial\psi}{\partial t}$, where $H = H^0 + H'(t)$. Simple algebraic simplification of the resulting expression leads to

$$c_aH'|\psi_a\rangle + c_bH'e^{-i\omega_0t}|\psi_b\rangle = i\hbar\dot{c}_a\psi_a + i\hbar\dot{c}_be^{-i\omega_0t}|\psi_b\rangle$$

where $\dot{c}_a$ and $\dot{c}_b$ stand for $\frac{\partial c_a}{\partial t}$ and $\frac{\partial c_b}{\partial t}$, respectively.

From here, we take inner products with each eigenstate individually, to yield two differential equations for c_a and c_b:

$$\dot{c}_a = \frac{-i}{\hbar}[c_a H'_{aa} + c_b e^{-i\omega_0 t} H'_{ab}]$$

$$\dot{c}_b = \frac{-i}{\hbar}[c_a e^{i\omega_0 t} H'_{ba} + c_b H'_{bb}]$$

where $H'_{ij} = \langle \psi_i | H' | \psi_j \rangle$.

Solution of these equations is difficult without making a few reasonable assumptions. First, we assume that the wavefunction is that of an electron around a stationary nucleus. Second, we assume that the time-dependent part of the Hamiltonian is of the form $H' = -qE_0 z\cos(\omega t)$, which describes a periodic electromagnetic wave linearly polarized in the z-direction interacting with a stationary charge q. This leads to a form for H'_{ij}: $H'_{ij} = -q\langle \psi_i | z | \psi_j \rangle E_0 \cos(\omega t)$. Second, we assume that the wavelength of the light is much larger than the size of the system, so that the system only sees the time-variance of the field, and not the spatial variance. One further simplification involves the expectation value of z: since the Hamiltonian commutes with the parity operator, the eigenfunctions of the Hamiltonian are either even or odd. Consequently, the expectation value of z corresponds to an integral of an odd function over all space, which is zero. Thus, we assume that the diagonal matrix elements of H' are zero in this case. These assumptions simplify the differential equations significantly, leading to the results

$$\dot{c}_a = \frac{-i}{\hbar} c_b e^{-i\omega_0 t} H'_{ab}$$

$$\dot{c}_b = \frac{-i}{\hbar} c_a e^{i\omega_0 t} H'_{ba}$$

Even with these simplifications, it falls to perturbation theory to solve these equations. However, Rabi came up with another approximation, called the rotating wave approximation, which allows exact solution of these differential equations [28]. One way to express the approximation involves a simplification of the form of H' [28]. This approximation simplifies the forms

of H'_{ab} and H'_{ba}:

$$H'_{ab} = \frac{V_{ab}}{2} e^{i\omega t}$$

$$H'_{ba} = \frac{V_{ba}}{2} e^{-i\omega t}$$

where $V_{ba} = -2qE_0\langle\psi_b|z|\psi_a\rangle$.

This simplification puts the differential equations for the complex amplitudes into a form which is analytically solvable, and requires no reliance on the time-dependent Hamiltonian being small enough to be considered a perturbation. In fact, this solution allows complete population transfer between the two levels. We now start from the simplified differential equations

$$\dot{c}_a = \frac{-iV_{ba}}{2\hbar} c_b e^{i(\omega-\omega_0)t}$$

$$\dot{c}_b = \frac{-iV_{ab}}{2\hbar} c_a e^{-i(\omega-\omega_0)t}$$

We then differentiate each of the above equations with respect to time, and substitute the original equations where possible to get two second-order differential equations:

$$\ddot{c}_b + i(\omega-\omega_0)\dot{c}_b + \frac{|V_{ab}|^2}{4\hbar^2} c_b = 0$$

$$\ddot{c}_a - i(\omega-\omega_0)\dot{c}_a + \frac{|V_{ab}|^2}{4\hbar^2} c_a = 0$$

These differential equations are easily solvable using Laplace transforms. Starting from the above differential equations, we define the following transforms: $C_A(s) = \mathcal{L}\{c_a(t)\}$; $C_B(s) = \mathcal{L}\{c_b(t)\}$. If we assume that we start in the state $|\ \psi_b\rangle$, we know that $c_b(0) = 1$, $\dot{c}_b \propto c_a(0) = 0$. We make some substitutions for simplicity also: $i(\omega-\omega_0) = \beta$, $|V_{ab}|^2/4\hbar^2 = \gamma$. From there, Laplace transforms of the differential equations lead to:

$$s^2 C_B - s c_b(0) - \dot{c}_b(0) + s\beta C_B - \beta c_b(0) + \gamma C_B = 0$$

$$s^2 C_A - s c_a(0) - \dot{c}_a(0) - s\beta C_A + \beta c_a(0) + \gamma C_A = 0$$

Substitution of the known initial values leads to:

$$s^2 C_B - s + s\beta C_B - \beta + \gamma C_B = 0$$

$$s^2 C_A + \frac{iV_{ba}}{2\hbar} - s\beta C_A + \gamma C_A = 0$$

Simple algebraic manipulation leads to:

$$C_B = \frac{s+\beta}{s^2+\beta s+\gamma}$$

$$C_A = \frac{-iV_{ba}}{2\hbar}\frac{1}{(s-\beta/2)^2+(\gamma+\beta^2/4)}$$

By completing the square and applying the inverse Laplace transform, we find that the complex amplitudes take the form

$$c_a = \frac{iV_{ba}}{2\hbar\omega_L} e^{i(\omega-\omega_0)t/2}\sin(\omega_L t)$$

$$c_b = e^{-i(\omega-\omega_0)t/2}[\cos(\omega_L t) + \frac{i(\omega-\omega_0)}{2\omega_L}\sin(\omega_L t)]$$

where ω_L is

$$\omega_L \equiv \frac{1}{2}\sqrt{\frac{|V_{ab}|^2}{\hbar^2}+(\omega-\omega_0)^2}$$

To further simplify this, we notice that, when detuning $\delta \equiv (\omega-\omega_0) = 0$, ω_L approaches $\frac{|V_{ab}|}{2\hbar}$, which we designate the "idealized Rabi frequency," Ω. With this substitution, the form of the amplitudes becomes

$$c_a = \frac{i}{\sqrt{1+(\delta/\Omega)^2}} e^{i(\delta)t/2}\sin(\omega_L t)$$

$$c_b = e^{i(\delta)t/2}[\cos(\omega_L t) + \frac{i(\delta)}{\omega_L}\sin(\omega_L t)]$$

Thus, we see that, as detuning increases, Rabi frequency increases, and the population transfer is incomplete. Experimentally, we generally use a continuous-wave source with a well-defined frequency tuned almost exactly to resonance in order to completely transfer the population. These equations further simplify to a compact matrix form:

$$\hat{R} = \begin{pmatrix} e^{i\delta t/2}\left[\cos(\omega_L t) - \frac{i\delta}{\sqrt{\Omega^2/+\delta^2}}\sin(\omega_L t)\right] & \frac{i}{\sqrt{1+(\delta/\Omega)^2}} e^{i\delta t/2}\sin(\omega_L t) \\ \frac{-i}{\sqrt{1+(\delta/\Omega)^2}} e^{-i\delta t/2}\sin(\omega_L t) & e^{i\delta t/2}\left[\cos(\omega_L t) - \frac{i\delta}{\sqrt{\Omega^2+\delta^2}}\sin(\omega_L t)\right] \end{pmatrix}$$

$\hat{R}$ is a Rabi operator, which operates on the wavefunction in vector form:

$$|\psi\rangle = \begin{pmatrix} c_a \\ \\ c_b \end{pmatrix}$$

For a given time t, the probability of population transfer as a function of frequency follows:

$$P_{trans} = \frac{\sin^2(\sqrt{\Omega^2 + \delta^2}t/2)}{1 + (\delta/\Omega)^2}$$

For our experimental purposes, we call the quantity $2\omega_L t$ the Rabi angle, since the Rabi operator has the same form as a rotation matrix. From a purely practical standpoint, for an electric field of constant magnitude, the Rabi angle is proportional to the time the Hamiltonian is applied, and proportional to the magnitude of the electric field. The phase of the $e^{i\delta t/2}$ term is important when multiple pulses are used without measurement in between, but in practice, its effects are usually eliminated by adjusting the phases or time delays of subsequent pulses so that the phase angle is some known function.

In order to implement Rabi oscillations in our system, we first find the correct frequency by scanning the frequency of our microwaves while applying a microwave pulse of set duration to the ion. We measure the probability of excitation of the ion, and see a curve which looks like Fig. 2.7. The form of the curve is a sinc^2 function of detuning, so we find the highest peak and set the microwave frequency to that feature. Once the proper frequency is found, Rabi oscillations of varying angles can be generated by modulating the time the microwaves are applied. By setting our detuning very close to zero, we ensure the population transfer is complete.

For a single trapped ion with two states $|\uparrow\rangle$ and $|\downarrow\rangle$, we usually note two pulses of particular importance: a $\pi/2$ pulse and a π pulse. The $\pi/2$ pulse is a pulse which takes an energy eigenfunction and transforms it into a 50/50 superposition of both eigenfunctions. A π pulse takes an energy eigenfunction and transforms it into the other eigenfunction.

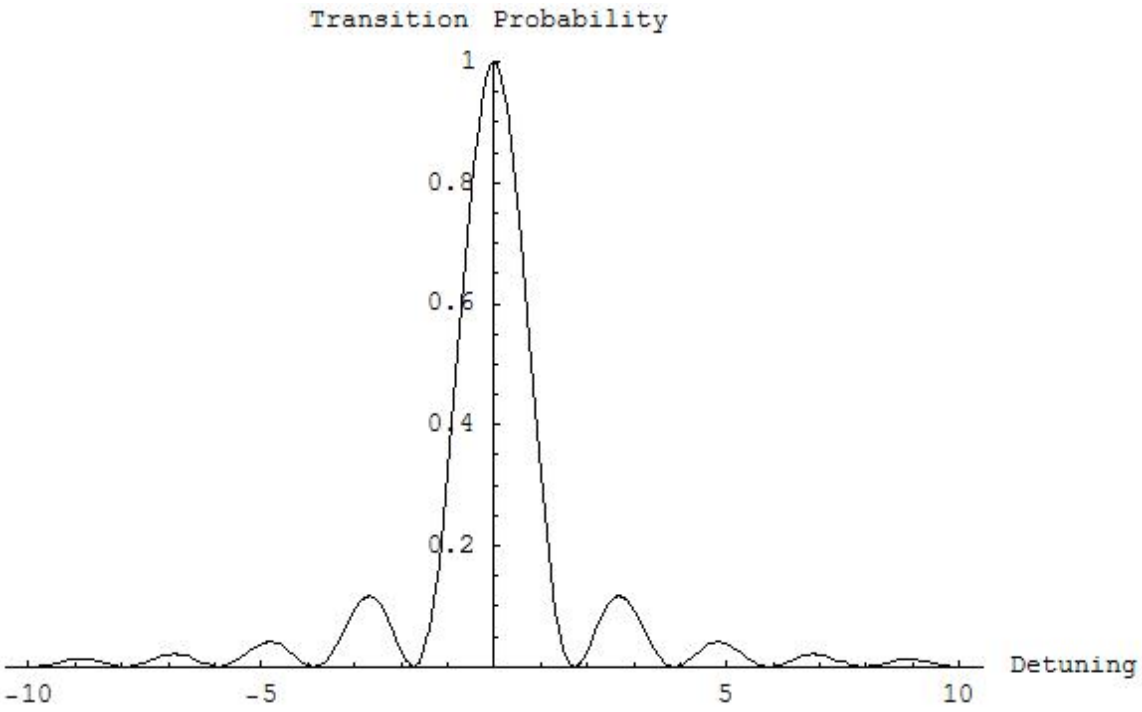

Figure 2.7: A curve illustrating how we find the center frequency to drive Rabi oscillations in our system. If we apply the microwaves to the system for a constant time and vary the frequency of the microwaves, we see the population transfer as a function of detuning follow a sinc^2 function. If we set the frequency to the center of the highest peak, we minimize detuning and ensure that population transfer between the two states is complete.

The truth table for a series of $\pi/2$ pulses is as follows:

$$|\uparrow\rangle \rightarrow \frac{|\uparrow\rangle + |\downarrow\rangle}{\sqrt{2}}$$

$$|\downarrow\rangle \rightarrow \frac{|\downarrow\rangle - |\uparrow\rangle}{\sqrt{2}}$$

For excitation with continuous-wave (cw) light, the time of the application can be varied to achieve any desired Rabi angle. However, mode-locked pulsed-lasers have a set pulse length which is not easily variable. Therefore, in pulsed-laser Rabi excitations, the time cannot be varied, so the energy must be varied instead. Since the energy in an electric field is proportional to $\vec{E}^2$, the Rabi angle is proportional to the square root of the pulse energy. The proportionality constant is determined by the characteristics of the laser pulse.

For energy levels with long lifetimes, slow excitation by cw light is sufficient to drive Rabi transitions, but for short-lived energy states, cw excitation is not sufficiently fast to excite the system. In such cases, ultrafast excitation is necessary to drive transitions much faster than the lifetimes of the corresponding states. For example, in our system, the $P_{3/2}$ energy state has a lifetime of order nanoseconds, so excitation must occur much faster.

2.5 The Ramsey Experiment

The Ramsey experiment is a very powerful multiple-pulse experiment which can provide a great deal of information about the system. In a Ramsey experiment, the system is prepared into a prescribed state and a pulse train is applied. This pulse train begins and ends with a standard $\pi/2$ pulse, and the delay between them, the pulses between them, and their relative phase can be adjusted. Simply put, the first $\pi/2$ pulse puts the system into a superposition, and, without anything in between, the second pulse, if it has the right phase, will put the system into one of the two eigenstates.

Inserting additional pulses will, of course, change the system. Studying the effect of the second $\pi/2$ pulse can provide information about the quantum state of the system. The population of the system versus phase of the second pulse is generally measured. This plot

of population versus phase angle will generally be sinusoidal, and is commonly referred to as Ramsey fringes.

The sinusoidal nature of the plot comes from the form of the Rabi operator; starting from a known state $|\uparrow\rangle$, the first $\pi/2$ pulse converts the system to $\frac{1}{\sqrt{2}}(|\uparrow\rangle + |\downarrow\rangle)$. Without anything between the two pulses, the system acquires a relative phase between the two states based on their energy splitting and the time between pulses: the state becomes $\frac{1}{\sqrt{2}}(|\uparrow\rangle + e^{i\omega_0 t}|\downarrow\rangle$, where ω_0 is the frequency splitting between the two states and t is the time between pulses. When the second pulse arrives, if it has the right phase, it will add constructively to the first, putting the system into the $|\downarrow\rangle$ state. The final population of the system in $|\downarrow\rangle$ goes as $\cos^2(\omega_0 t - \phi)$ where the phase is designated ϕ. When the relative phases match, the pulses constructively interfere. When they are 180 degrees out of phase, the pulses interfere destructively, returning the system to the $|\uparrow\rangle$ state.

Adding additional pulses between the two $\pi/2$ pulses in a real system can have a variety of effects on the population. The additional pulses could act on the system in the same way as the Rabi pulses, in which case one would see a shift in the phase of the Ramsey fringes. However, the additional pulses could couple the system to different energy levels, affecting the amplitude of the Ramsey fringes. In our experiment, we use microwave $\pi/2$ pulses to put the ion into a superposition of $S_{1/2}$ hyperfine states and use optical pulses between the two microwave pulses to excite transitions between the $S_{1/2}$ and $P_{3/2}$ states. The optical pulses have effects on both the contrast and phase of the Ramsey fringes, as will be discussed in chapter four.

Chapter 3

Apparatus

In this chapter, the specifics of the experimental apparatus are discussed. First is a brief discussion of the ion traps used in the experiment, followed by discussions of the laser systems used to control the ion. Brief treatments of second-harmonic generation, cw laser locking, and ps pulse picking are given. Finally, the electronic elements which control the experiment are explained.

3.1 Linear Ion Trap

Our system uses linear Paul traps in order to be able to hold and control multiple ions. As opposed to the simple quadrupole trap, which has a point radiofrequency node, the linear Paul trap has no confinement in one axis, resulting in a linear radiofrequency node. In a simple quadrupole trap, the fact that there is only one rf node means that it is impossible to eliminate the micromotion for all of the ions, making control impossible. The linear Paul trap solves this problem by providing a linear rf node for the ions to line up along, restricting the ions to a number of essentially static sites on a line. This simplifies illumination, detection, and imaging greatly. In our system, (and in any real system) the linear rf node does not extend to infinity, but is instead capped at the ends, providing weaker confinement in the axial direction (rather than no confinement).

The fields we use are well-approximated by a three-dimensional harmonic potential when the ions are near the center of the trap. The frequency of the trap is about the same for two axes,

with the third axis much less strongly confined. Doppler cooling crystallizes the ions, keeping them lined up along the rf node. Experiments in this system begin with an initialization to the dark state, and cooling is performed just before the state is initialized. Therefore, the ions are kept at too low a temperature to move out of the sites on the linear node while we perform an experiment. We set up the imaging system to measure the photons they emit on photomultiplier tubes and a CCD camera.

3.2 Radiofrequency Resonator

In order to actually have decent trapping strengths, rf voltages on the order of several hundred volts must be generated and applied to the rf electrodes. The rf generators we use can generate several watts of rf power, but the output impedance of the devices is generally 50Ω. RF voltages on a line with known impedance and known average power input are related by $P = \frac{V^2}{R}$, where P is average power in watts, V is rms voltage, and R is resistance in ohms. For a given power, it is advantageous to increase the impedance in order to acheive higher voltages. Since the trap is essentially an open circuit, it has very high characteristic impedance, but if the source and trap are not matched, most of the power will be reflected.

In order to transmit all the power to the trap, we use a helical resonator to match impedances. A helical resonator consists of a copper can with two coils in it, one to couple in low-impedance rf and one to output a high-voltage, high-impedance signal. Theoretically, the problem of a helical resonator is more complicated than that of the simpler coaxial resonator, but the basic concept is the same. The length of the coil is matched to approximately a quarter-wavelength, and a standing wave is generated, with the input coil at the low-electric-field end of the wave and the output at the high-electric-field end. Energy is stored in the electric field inside the can, and losses occur in the skin of the copper. A common measurement to characterize a resonator is the Q-factor, which is defined as the energy stored in the resonator divided by the energy lost per cycle $Q = \omega U / P_{losses}$. Since the energy stored is proportional to the volume of the resonator and the losses are proportional to the surface area of the can and wires, it is

generally seen that larger resonators have larger Q-factors.

3.2.0.1 Resonator Design

Helical resonators have been well-characterized, providing a great deal of insight regarding their design and construction [29]. When designing a resonator, the first important parameter is the resonant frequency. The resonant frequency of the unloaded resonator (with just an open circuit at the output) is denoted by f_0. An important point is that everything connected to the output is also part of the resonator, so, for example, connecting large capacitive loads to the output of the resonator will affect its performance. For our purposes, the linear Paul trap is a small capacitive load of order picofarads. Even with this small load, the resonant frequency with the trap connected can fall as low as $f_0/2$. Correcting for this, we start by choosing an appropriate f_0, in MHz.

After choosing f_0, we also note the inner diameter of the copper pipe we will use to make the can. This parameter is D. We perform all measurements for the resonators in inches, which are the same units as those used in [29]. Our choice of D restricts our choice of coil diameter d such that $0.45 \leq d/D \leq 0.6$. We are additionally restricted in that the axial length of the coil, b is related to the diameter in such a way that $b/d > 1$. The ratio b/d determines the valid range of the wire diameter d_0 to the pitch per turn of the coil, τ. For $b/d \sim 1.5$, $0.4 \leq d_0/\tau \leq 0.6$. For $b/d \sim 4.0$, $0.5 \leq d_0/\tau \leq 0.7$. Further, the axial length of the coil determines the range of acceptable lengths for the can itself (B), as $B \approx (b + D/2)$.

Putting all of the restrictions together, as well as some equations describing the inductance and capacitance of a helical coil, it can be determined that the range for the number of turns in the coil per inch (n) is

$$n_{\pm} = \frac{1720}{f_0 D^2 (b_{\mp}/D)(d_{\mp}/D)^2} \sqrt{\frac{\log_{10}(D/d_{\mp})}{(1-(d_{\mp}/D)^2)}}$$

where d_- and d_+ are the minimum and maximum values allowed for d based on D, and b is the axial length of the coil. The number of turns n can then be used to determine the range of wire

thicknesses based on the range of d_0/τ: $0.4 \leq d_0 n \leq 0.6$ From that restriction, a wire thickness is chosen, and the pitch is chosen such that the pitch ratio falls in the above range.

With D, f_0, d_0, and d_0/τ chosen, we next calculate the number of turns we need via $N = 1900/f_0 D$. With known pitch and number of turns, we calculate the axial length of the coil easily: $N\tau$. Once the wire size, number of turns, and axial length are known, it is simply a matter of winding the right coil.

In practice, the requirements for building a working resonator are more relaxed than the calculations would suggest. For example, pitch ratio of the wire d_0/τ is not particularly important, so long as the wire fits. In other words, the wire can be widely spaced without sacrificing functionality. Pitch ratios of 0.2 and 0.25 have worked well. Moreover, the paper suggests an optimal ratio of coil length to width (b/d)of 1.5, but larger ratios of approximately 2 or 3 have worked as well.

3.2.0.2 Resonator Construction

The major components of a resonator are a copper pipe of the required length and diameter and two caps. One cap will be designated the low-voltage end, and will need an rf connector in its center, where the input coupler will be connected. On the output end, a hole must be drilled in the center that is large enough that at least two wires can go through with a few millimeters of space between them. Another hole is needed off-center for an rf connector, where the grounding wire will be connected.

In order to permit the use of bias voltages on the resonator, the low-voltage end of the coil is connected to an rf connector leading out the side of the can, with the outer conductor shorted to the can. This way, it is possible to bias the output to any desired DC voltage. Similarly, another rf connector is placed at the off-center hole on the high-voltage cap and connected to a wire (the rf grounding wire) that is fed out the center hole. The rf grounding wire can also be grounded or biased to any static voltage. The other end of the coil is also fed out via the center hole. The two wires together provide an RF high-voltage output and an RF ground output.

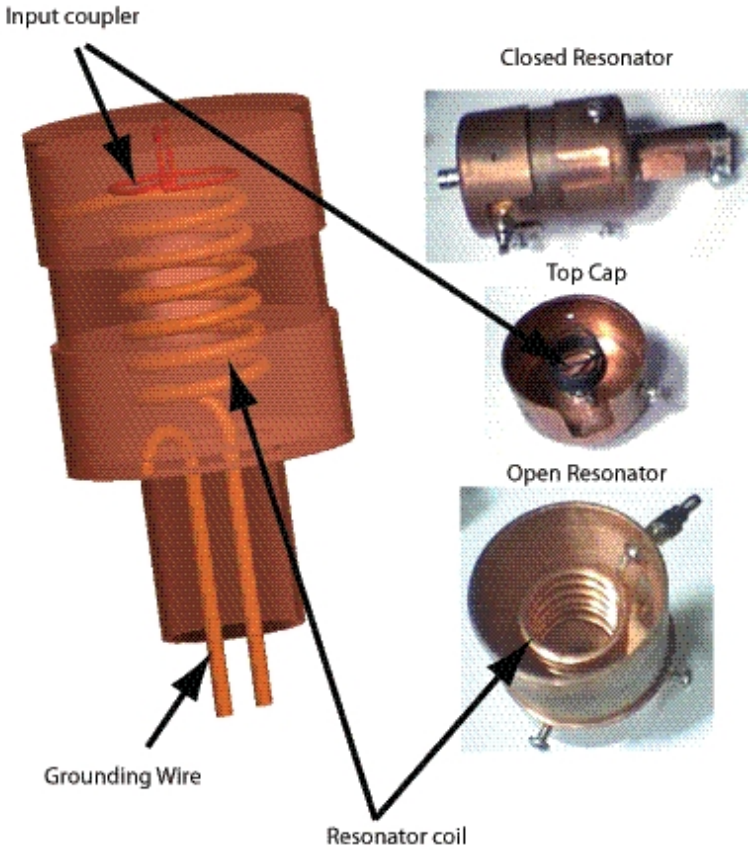

Figure 3.1: A picture of a helical resonator. The input coupler has rf applied to it. The resonator coil reacts, setting up a high-voltage oscillation, which ends up at the output, which is at high-voltage rf compared to the grounding wire.

In order to reduce losses in the resonator over time due to oxidation of the surface of the copper, one can gold-plate the copper parts in order to prevent oxidation. The solution used to gold-plate the copper is potassium aurocyanate in water. The primary dangers of the solution involve the fact that it contains cyanide, and therefore is potentially a fatal toxin. Care is required in two ways: first, it is important that the solution does not make contact with skin, and second, the solution must not be exposed to acid in any form. Acid reacts with potassium aurocyanate to develop hydrogen and cyanide gases. The former is explosive, the latter highly toxic. Work with potassium aurocyanate should be performed under a fume hood which contains no acid.

Once the necessary precautions are taken, gold-plating the copper is simple. There are two ways to plate the pieces. First, one can connect the anode of a voltage supply (set between eight and ten volts) to the copper piece, put the cathode in the solution, and dip the copper parts into solution. The voltage supply will draw current, and gold will be plated onto the copper. Alternately, it is possible to connect the cathode to a metal hemostat and grip a piece of absorbent material soaked with the solution. Then gold can be "painted" onto the copper piece (still connected to the anode). This method is a bit more time-consuming, but ultimately uses up less of the solution and only coats the desired surfaces. Once the pieces are plated, they can be connected, and all that is left is to couple rf into the resonator.

3.2.0.3 In-coupling and Q

Inductively coupling rf into the resonator requires another, smaller coil across which low-impedance rf can be applied. The diameter of the in-coupler is generally about half that of the resonator coil, and only one or two turns are usually required. This coil is connected to the BNC on the low-voltage cap and grounded to the surface of the can. The low-voltage cap is connected to the can in such a way that it can move freely along the axial direction with a range of a few millimeters. Moving the cap changes the coupling between the input and output coils, which must be adjusted to allow the rf to go through the resonator without reflection.

Once the low-voltage cap is connected, it is useful for in-coupling to connect the output to something with similar characteristics to the trap it will eventually be connected to. The trap itself is almost an open circuit, but it is surrounded on all sides by a grounded stainless steel vacuum chamber. Therefore, it is usually fine to simply surround the output wires with a metal can, which provides a nearby ground as in the trap.

Next, it is necessary to connect rf to the resonator. The simplest way to determine the quality of the in-coupling is to measure the rf reflected from the in-coupler. Connecting a the rf to the resonator through a directional coupler and connecting the reflected signal to an oscilloscope is the easiest way to measure the back-reflected signal. If everything is connected properly, a sudden dip in the amplitude of the reflected signal should occur near the expected frequency (usually around half of the chosen f_0). The amount the amplitude changes depends on the quality of the in-coupling. In order to fine-tune the in-coupler, the input frequency can be modulated while the position of the in-coupler is adjusted. At some point, a minimum in the amplitude of the reflected signal should be found, where moving the coil in any direction results in an increase of the minimum amplitude of the reflected signal. In addition, the minimum amplitude of the reflected signal should be small, of order 100 times smaller than the maximum reflection far from resonance. If a minimum is not found, the in-coupler can be coarsely adjusted by cutting off or adding a turn, or by changing the diameter of the in-coupler. If the minimum reflection was found with the cap pulled out as far as possible, remove a turn of the coil or make it smaller. If the minimum occurs when the cap is pushed in as far as possible, adding a turn or increasing the size of the in-coupler can solve the problem.

Once the in-coupling is good, the low-voltage cap can be secured to the rest of the can and the Q can be measured. As previously discussed, Q is a unitless quantity which is defined by the amount of energy stored per by the resonator divided by the losses per cycle. Directly measuring those quantities is difficult, however, so an alternate method of measurement is required. The simple quantities which can be measured instead are the full-width half-max (FWHM) of the

reflected power spectrum and the resonant frequency. The Q can also be expressed as

$$Q = \frac{f_0}{FWHM}$$

where f_0 is the actual resonant frequency, where the reflection is minimized, and the $FWHM$ is the full-width-half-max of the resonance, in the same scale as f_0. The width required is the FWHM of the reflected power spectrum, so it is necessary either to measure power or to square the amplitude. In the amplitude scale, the points of interest are the points where the amplitude is $1/\sqrt{2}$ (≈ 0.707) of the full amplitude far from resonance. Measuring these quantities allows simple calculation of the Q.

For most resonators, the Q depends on the width of the pipe used, which serves as a sort of characteristic length. Resonators made with 2-inch pipe have been found to commonly have Q's of a few hundred. 3-inch pipe commonly results in resonators with Q's above 500. Larger pipes should result in higher Q, simply because of the aforementioned relationship between the energy stored and losses. Energy stored is proportional to volume ($\sim d^3$) and losses are proportional to surface area ($\sim d^2$), so the overall Q factor is roughly proportional to the diameter of the resonator.

Once the Q is measured, the trap is ready to be connected to the trap. Small adjustments of the in-coupling are always necessary when the system is changed, but the resonance should be close enough that further modifications of the in-coupler should be unnecessary. Once the in-coupling is fine-tuned, the resonator is usually stable enough to work continually for months without any adjustment.

3.3 Continuous Wave Diode Laser

In order to provide our continuous-wave (cw) excitations, we use an amplified external cavity diode laser built by Toptica which emits cw light at approximately 858 nm. This wavelength is four times the wavelength of the $S_{1/2}$ to $P_{3/2}$ transition of the ion. The electronic structure of the different isotopes of cadmium is shifted by several hundred MHz for each iso-

tope, but the laser is tunable over this range, so the structure of any isotope of cadmium is accessible. The laser diode shines onto a grating which forms a cavity with the diode. The cavity outputs a small amount of cw infrared laser light, which is mode-matched into a tapered amplifier to achieve powers of about a watt.

The frequency of the laser is tuned by adjusting the position of the grating with respect to the diode via control of a piezoelectric element connected to the grating. By adjusting the position slightly, the characteristics of the diode-grating cavity are changed in such a way that the frequency is continuously tunable over ranges of approximately 0.02 nm. Larger shifts result in changes in the dominant cavity mode or mode competition. Fortunately, the resonances of all stable isotopes of cadmium lie across a range of less than 0.01 nm, such that the full tuning range is almost never required.

The laser diode is highly sensitive to changes in its environment, so its current and tenperature are controlled by a series of electronic modules supplied with the laser. The temperature is controlled by a servo system and is generally held at about room temperature. The current is kept stable at about 90 mA.

3.3.1 Higher-harmonic Generation

Once sufficient power is generated in the infrared, the light must be frequency-doubled twice to excite the ion. Efficient frequency-doubling of cw light requires construction of a cavity and insertion of a non-linear material, which has a polarization component proportional to the square of the electric field. In our case, the non-linear material is a crystal of potassium niobate for doubling infrared and a BBO crystal for doubling blue. The input coupler ideally transmits about as much light as is lost in one roundtrip of the cavity (about 1%) in the principal frequency, and the nonlinear crystal is placed in the path of the light through the cavity. In this way, light of the principal frequency is built up in the cavity, resulting in increased laser intensity on the nonlinear crystal. The nonlinear crystal sees a high-intensity electric field, and polarizes with significant contributions from $\vec{E}^2$. The square of a sinusoid is another sinusoid with twice the

frequency and a DC offset, so polarization proportional to twice the laser frequency is set up. This polarization generates light at twice the principal frequency, with efficiency of about 25%. The output coupler is designed to pass light of this frequency, so the final result is a laser beam with twice the frequency of the first and about 1/4 the intensity.

The same procedure is repeated with optics designed to reflect blue but pass UV, and with a non-linear BBO crystal designed to double blue light. The final result is between several hundred microwatts and a few milliwatts of laser light at 214.5 nm which can be used to drive transitions of the ion. In the end, the ultraviolet light is commonly split into two branches, one σ^+ polarized to cool and illuminate the ion, and one π polarized to pump the ion to the dark state. The beams are switched on and off by acousto-optic modulators (AOMs), which shift the frequency and direction of the laser when it passes through a crystal with an acoustic wave present in it.

3.3.2 Tellurium Lock System

The most commonly used isotope for experiments is ^{111}Cd. The resonance from the $S_{1/2}$ state to the $P_{3/2}$ state is at about 858.0261/4 nm, but drifts in the unlocked diode laser system are of the order 0.0005 nm, or on order of several hundred megahertz. Moreover, the absorption line for cadmium is only 60 MHz wide, so keeping the laser on the red side of that line requires long-term stability to around a few MHz. This stability requirement means that the laser needs to be stabilized by some outside reference. In our case, it just so happens that there is a line in the absorbtion spectrum of Tellurium atoms at 429.0143, meaning that we can actively lock our laser frequency to that absorption line. The line is separated from our desired excitations by about 2 GHz, so the frequency of the laser is modulated by AOMs in the lock system as well as in the main beam lines.

In order to run the lock, a small amount of blue light is pulled from the main beam by a piece of uncoated glass, which reflects about 5% of the light incident on each surface. The reflection from the front surface is directed to the tellurium lock system. The absorption line

for $^{111}Cd^{+}$ is at one half of 429.0130 nm, which is a difference of about 2 GHz in the blue. This is countered in two stages: first, the main beam's frequency in the uv is upshifted by the AOMs which switch the beams on and off. Second, the picked-off blue light being sent to the tellurium lock is passed twice through another AOM which lowers its frequency. This downshifted beam is sent to the tellurium cell and associated optics in order to lock the signal.

The tellurium lock system operates on the same principle as a saturated absorption spectroscope. The tellurium occupies a small glass cell connected to a heat source at about 450 degrees Celsius, heated in order to increase the tellurium vapor pressure in the cell. The blue light is split into three beams: pump, probe, and reference, with the pump beam stronger than the other two by about an order of magnitude, and the other two having nearly identical intensities. The pump and probe beam are counter-propagating along the same path in the cell. The reference beam occupies a different space in the cell.

The pump beam strongly excites the transition in tellurium, resulting in a Doppler-broadened absorption spectrum in its intensity. The powerful pump beam excites any tellurium in its path which is properly doppler shifted to absorb the light, resulting in an apparent linewidth of a few gigahertz, which can be calculated from the expected Doppler shift of tellurium atoms moving at speeds equivalent to a temperature of several hundred degrees Celsius. The expected most probable velocity of tellurium atoms at 400 Celsius, for example, is $\sqrt{\frac{2k_BT}{m}}$, which for this case is 350 m/s, which corresponds to a frequency shift in the absorbed light of about 7 GHz.

However, since the probe beam counterpropagates along the same path as the pump beam, most of the atoms it would excite are already excited by the pump beam when the frequency is tuned to the tellurium line. As a result, the absorption spectrum of the probe beam has a characteristic sharp peak at the resonance, and this narrow line is clearly visible when the signal from the probe is subtracted from the reference signal. We lock to this narrow peak by dithering the frequency and using the resulting signal to control a servo. When everything is working correctly, the laser can be locked to the resonance of $^{111}Cd^{+}$with a linewidth of order

1 MHz, and can remain locked for hours without any difficulty. With this kind of stability, it is common to conduct experiments using this light for hours without adjusting the laser.

3.4 Mode-Locked Ti:sapphire Laser

The mode-locked Ti:sapphire laser we use is a Tsunami picosecond (ps) pulsed laser pumped by a ten-watt Verdi green laser at 532 nm. The green light drives a Ti:sapphire crystal to produce infrared light at a frequency determined by the laser cavity. The cavity has length of 3.6 meters, corresponding to the time delay between pulses(12 ns).

The center frequency of the laser is determined by the orientation of a birefringent filter in the laser cavity, but, since the pulse width corresponds to a transform-limited frequency bandwidth of $\sim$ 420 GHz, only rough tuning of the laser is necessary. However, the large bandwidth means the pulses excite all possible transitions separated by much less than the bandwidth. Individual addressing of close states becomes impossible.

For all practical purposes, we assume that the laser excites equally all transitions separated by frequencies much less than the pulse bandwidth. For example, since the hyperfine splitting is only 14.5 GHz, if we tune the laser so that its center frequency is roughly 858.02 nm (S-to-P transition), all of the possible couplings between all of the populated hyperfine levels in the $S_{1/2}$ and $P_{3/2}$ states are made. Fortunately, we can select which transitions can be made by adjusting the polarization of the laser light.

The intensity of the pulses generated by the laser when it is mode-locked has the shape of a sech^2 function, which, as previously described, affects the way the pulses interact with the ion. As previously discussed, the length of the pulses is not variable, so instead of varying the time we vary the power of the pulses. With the power as the variable, we expect to see the transition probability for a given pulse $P_{trans} = \sin^2 \theta/2$ vary with the square root of the power, as detailed on 21.

3.4.1 Pulse Picking

When properly mode-locked, the laser emits a pulse every twelve nanoseconds. In order to control these pulses, we use a pulse picker, which can pass a single pulse or a number of pulses. The pulse picker consists of an electro-optic modulator (EOM), which changes the polarization of the beam by ninety degrees when high-voltages are applied, and a beam splitter. When the EOM is on and properly aligned, it rotates the polarization of the beam, which is then directed onto a beam-splitter which reflects light polarized in one direction and passes light polarized orthogonally. With appropriate alignment of the device, light from the laser can be made to selectively reflect from or pass through the beam-splitter, effectively selecting pulses to be sent further in the experiment. The pulses not sent to the experiment are dumped into a beam stop. Control of the EOM is performed by electronics designed specifically for that purpose, which trigger from a signal generated when the laser emits a pulse and can control the EOM on the time scale of nanoseconds, allowing selection (or blocking) of single pulses. The pulse picker works in the infrared, where an extinction ratio between the picked and unpicked pulses was measured to be better than $100:1$. Since the output of the frequency doubling is proportional to the square of power, we expect the extinction ratio after the two doubling stages to be raised to the fourth power, resulting in an expected ratio of order $10^8:1$. The extinction in the ultraviolet was too great to be measured directly–the unpicked pulses were indistinguishable from the noise on the photodiode used to detect the pulses.

3.4.2 Higher-harmonic Generation from Pulses

The Tsunami does not generate pulses in the ultraviolet. Like the cw laser system, it emits pulses with one-fourth the optical frequency needed to excite transitions in cadmium. Therefore, we must frequency-quadruple the pulses, much as we do with the cw light. However, the buildup cavities necessary to achieve high efficiency in cw doubling are unnecessary in the ps pulse regime since the pulses already have extremely high peak intensity. For instance, the Tsunami may emit up to two watts of infrared light. However, the duty cycle of the laser is

extremely small; the pulses are a few picoseconds in length and they follow each other every 12 nanoseconds, resulting in a duty cycle of about $\frac{1}{100}^{\text{th}}$ of one percent, translating to peak powers of hundreds of watts, which are sufficient for frequency-doubling.

Since the peak intensity is so high, no buildup cavities are used to frequency-double the pulsed laser. Rather, the laser light is focused into a nonlinear crystal, and the result is a frequency-doubled laser pulse. The first doubling crystal is an LBO crystal, the second is a BBO much like the second cw doubler. After passing through both crystals, the light is directed to the trap.

3.5 Electronics

The experiment is run by a LabView program on a computer which is equipped to control TTL circuits which, in turn, control various electronic elements which generate the signals we need to perform experiments. The computer is equipped with a LabView-controllable card which sends TTL signals to logic circuits, switches, detectors, and frequency generators. The card is equipped with its own timing circuit which allows control on the scale of hundreds of nanoseconds. Most of the experimental apparatus connects with this card in some way.

For instance, the lasers are controlled by AOMs which, when turned on, direct light onto ions in the trap. The AOMs are driven by radiofrequency generators which are, in turn, controlled by switches connected to the TTL card. Population transfer between the hyperfine levels of the ion's ground state (separations of order MHz-GHz) are controlled by microwave generators which are controlled by the TTL card. The detectors count photons and send signals to the computer detailing the times photons arrive. Counting photons only at certain times is implemented by a gate circuit which only passes pulses when given an appropriate signal by the TTL card.

Much of the rf generation and control for the experiment is done by packaged electronics designed for those purposes. For example, the radiofrequency generation for the experiment is handled by numerous packaged generators, mostly from Hewlett-Packard. These devices can

emit phase-locked radiofrequency at frequencies from a few MHz to tens of GHz. Their outputs are controlled by packaged radiofrequency switches. Their outputs are amplified mostly by packaged rf amplifiers designed for given frequency ranges, though some amplifiers have been built from components by members of the group. The rf sources drive the AOMs and EOMs in the experiment, as well as directly exciting the ion with microwaves.

Detection is handled by two types of devices, a CCD camera and photomultiplier tubes (PMTs). The CCD camera is a device which gives information on the positions of photons measured on the detection surface. Its quantum efficiency is only a few percent, so it is best used to look at the shapes of bright sources. For example, it is useful in determining the configuration of the imaging optics; correctly aligned optics show a bright ion as a small, bright spot. Poorly aligned optics show corresponding drops in image quality, such as diffuse images and halos. For operation of the photomultiplier tubes it is important that the ion image be focused on the PMT (due to its limited size), so the CCD image is used as an indicator for correct alignment of the image onto PMTs.

Photomultiplier tubes have much higher quantum efficiency, and so are used when counting photons is required. They amplify a single photon event into a large signal by cascading photoelectrons between a series of surfaces held at high voltages with respect to one another. A photon colliding with the first surface generates a photoelectron, which is accelerated to the next surface to generate several more electrons, which are acclerated to the next surface, and so on. The end result is that PMTs have quantum efficiencies of better than 10%.

The electronics thus form a crucial element of the experiment, controlling lasers, microwave excitations, detection, and timing. However, most of the individual components, being manufactured pieces, are usually treated as controllable and well-characterized black boxes. Together, they form a framework which allows control of cw lasers and microwave beams on time scales of hundreds of nanoseconds, addition of sidebands to the laser frequency, time-resolved detection of photons with high efficiency, spatially-resolved detection of photons with reasonable efficiency, and many other actions vital to the conduction of the experiment.

Chapter 4

Experiment

In this chapter, the experimental procedures used and measured data are presented. In the first section, the pulsed-laser Rabi experiment is discussed, in which ps pulses were used to excite the S-to-P transition in an ion. The second section details our pulsed-laser Ramsey experiment, in which we surrounded the ps pulses with a Ramsey interferometer to measure the coherence of the ps transtions. In addition, we found a way to accurately measure the hyperfine splitting of the P state with these ps pulses, by measuring the phase of the restored Ramsey fringes.

4.1 Pulsed Laser Rabi Experiment

Of the two experiments discussed here, the first was a simple application of the pulsed laser to an ion in order to drive transitions between a pair of states in a single trapped $^{111}Cd^{+}$. The states chosen were the $S_{1/2}$ and $P_{3/2}$ states. The pulsed laser was tuned to approximately 858.02 nm, frequency-quadrupled, and sent through polarizers in order to achieve π polarization, and the cw laser was set up as previously discussed. The apparatus is shown in Fig. 4.1.

The experiment was designed to show that ultrafast pulses are capable of controllable excitation of single ion states. By exciting the ion with the pulsed laser, we expect to see oscillations in the final state population density of the ion which can be measured by averaging the ion's brightness over a number of runs. Excitations from the $S_{1/2}|0,0\rangle$ (dark) state to the $P_{3/2}|1,0\rangle$ state result in spontaneous emission with lifetime 2.647 ns [6]. The emitted photon

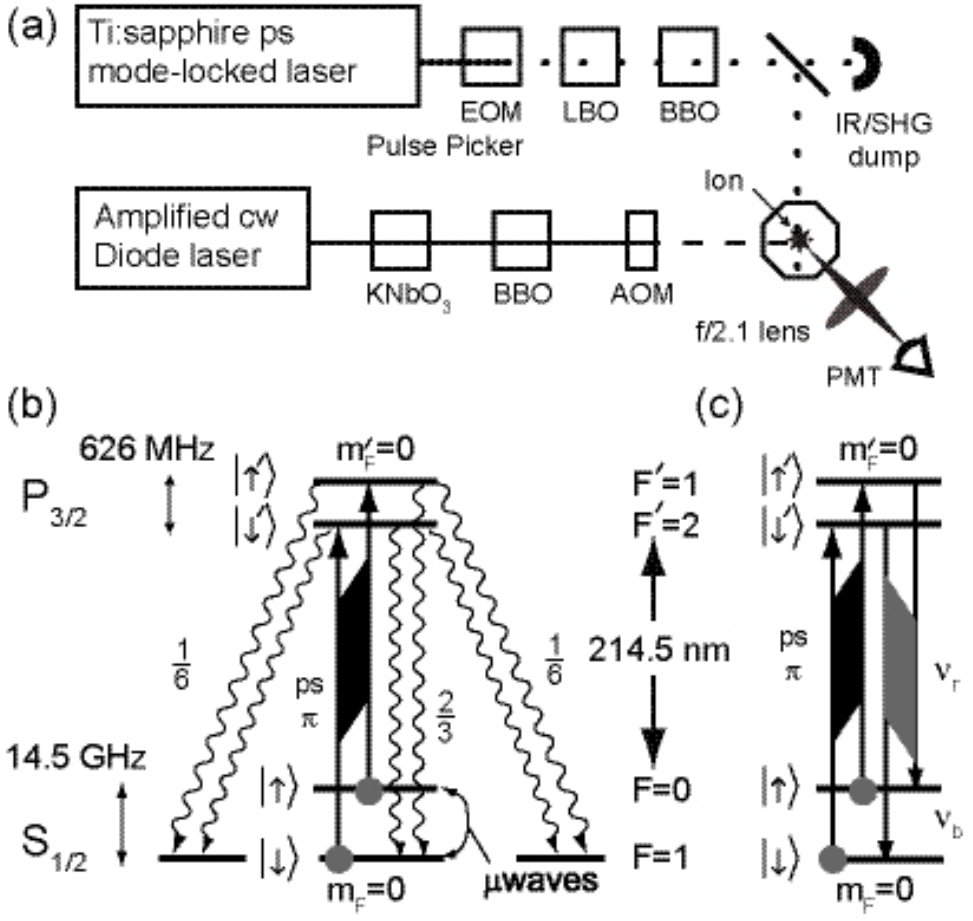

Figure 4.1: A diagram of the experimental apparatus and a few key transitions in the experiment. (a) A diagram of the experimental apparatus. Cw light from the Toptica is frequency-quadrupled and split into two beams, one which serves to cool and detect and another used to optically pump to the dark state. The cw beams are controlled by AOMs. Light from the pulsed laser is sent through the pulse picker with extinction in the IR of better than 100: 1, then frequency-quadrupled and directed onto the ion. The pulse picker is controlled by pulses from the computer. (b) The relevant transitions for the PL Rabi experiment. Excitation via an ultrafast pulse from the dark state sends the ion to an electronic state which can decay with known probability (1/3) to the bright state. (c) In the two-pulse experiment, when laser intensity corresponds to about a π pulse, the ion population density is transferred up to the $P_{3/2}$ state by the first pulse, and partially de-excited by the second pulse, assuming spontaneous emission has not already occurred.

can have one of two frequencies, as the ion's electronic state can decay to several different states. The fluorescence branching ratios state that the ion has a probability of decaying back to the $\mid 0,0\rangle$ state of 2/3, but it can also decay to the states $\mid 1,1\rangle$ and $\mid 1,-1\rangle$, each with a probability of 1/6. Fortunately, the $\mid 1,m_F\rangle$ states are all equally bright when exposed to the cw detection beam, which results in a final state of the ion brightness such that the probability of the ion being measured in the dark state is proportional (with a factor of 1/3) to the probability it was excited to the $P_{3/2}$ state.

$$P_{bright} = \frac{1}{3}\sin^2(\theta/2)$$

Here, θ is the Rabi rotation angle of the laser pulse, with $\theta/2 = a\sqrt{E}$, where E is the energy of the laser pulse ($E = P * t_{duty}$ P = average power, t_{duty} = duty cycle) and a is a constant factor determined by the characteristics of the beam incident on the ion. In our case, the factor a was determined from the data as the single parameter of a fit.

In the experiment, we begin by initializing the ion state to the dark state. This is performed in two steps. First, the cooling beam is modulated with the EOM to optically pump any population *out* of the dark state, and cool it to the Doppler limit. After a few hundred microseconds, the ion is cool and it is pumped to the dark state with the π polarized cw beam, which pumps the ion to the $\mid 0,0\rangle$ state in a few tens of microseconds. The pump time is determined beforehand by measuring the brightness as a function of pump time, and a time is selected that is long enough that the ion becomes completely dark (several tens of microseconds). Once these two stages of optical pumping are complete, the ion is initialized to the $S_{1/2}|0,0\rangle$ state and ready for manipulation.

In order to excite the ion from the $S_{1/2}$ state to the $P_{3/2}$ state, a single picosecond pulse is directed onto the ion. The energy of this ps pulse is controlled by a half-wave plate in the infrared. The half-wave plate rotates the polarization of the beam as it enters the doubling crystal, and, since the doubling crystal only works with one direction of polarization, the light polarized in the wrong direction is not doubled, effectively attenuating the laser in the UV.

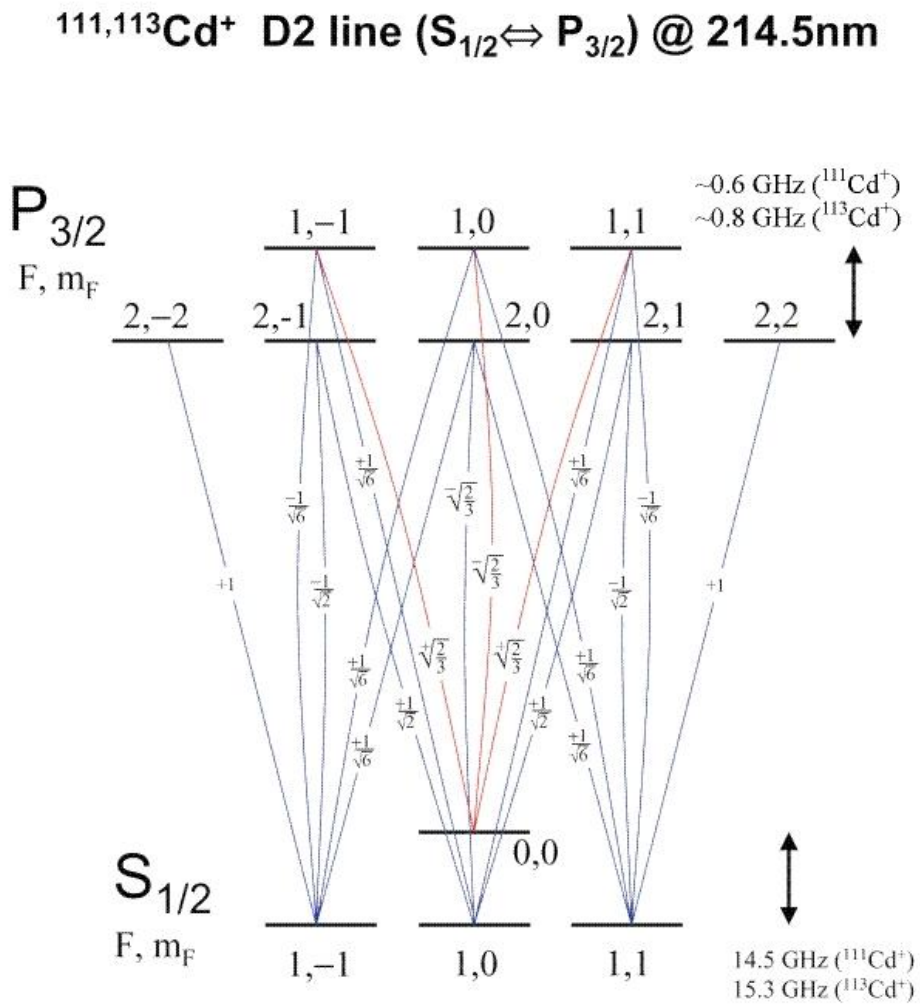

Figure 4.2: A diagram of the allowed transitions between the $5p\ ^2S_{1/2}$ and $5p\ ^2P_{3/2}$ states, and their branching ratios. Note that the allowed transitions from the $|\ 1,0\rangle$ state in the P manifold can decay to the dark state or the bright state. It has a 1/3 probability to decay to the bright state.

The polarization of the UV ps beam is selected to be π polarized, thus exciting transitions with $\Delta m_F = 0$. As previously stated, the expected effect of the laser pulse is a transition with probability $P_{\text{trans}} = \sin^2(a\sqrt{E})$, where P is the energy of the laser pulse. Once the pulse hits the ion, we wait for about 10 μs, which is much longer than the lifetime of the $P_{3/2}$ excited state. If excitation did occur, we expect spontaneous decay to the bright state with probability 1/3. Therefore, when we measure the brightness of the ion, we expect to see the ion in the bright state with probability $P_{\text{bright}} = (1/3)P_{\text{trans}}$.

We measure the ion's brightness with the σ^+ beam and repeat the experiment. For each energy setting of the pulsed laser, we recorded $60,000$ events, and fit the histogram of the number of events versus the photon counts to known bright and dark histograms. We took data for a number of different power settings and fit the resulting data for P_{bright} to $(1/3)\sin^2(a\sqrt{E})$, with a as the only free parameter. The fit gave $a = 0.42$ pJ$^{-1/2}$, which is comparable to an expression for a determined by geometric characteristics of the beam, $a_{\text{theory}} \approx 0.49$ pJ$^{-1/2}$. As a result of limited available laser power, we were only able to reach pulse energy equivalent to about a π pulse.

In order to achieve larger rotations of the state population, we placed a curved mirror to reflect and refocus the pulse on the ion. If the reflection were perfect and infinitely fast, we would expect to see the ion become half as bright and the rotation angle to increase twice as quickly. In this idealization, the first pulse rotates the state population by some angle, but the effect of the second depends on the first. Since the ion is moving around in the trap, the distance between the mirror and the ion is changing at the trap frequency. The motion of the ion extends over a few optical wavelengths, so we expect the ion to see a different relative phase between the two pulses in each experiment. As a result, the two pulses are coherent in each individual experiment, but over the course of a large number of experiments, the effect of the second pulse is essentially washed out when the first pulse is not about a π pulse (in which case the optical phase is irrelevant, and the second pulse will bring the population completely back down). The brightness of this idealized system as a function of pulse energy is $P_{\text{bright}} = (1/6)\sin^2(2a\sqrt{E})$.

In the end, we were able to achieve rotation angles of greater than π, but, due to imperfect transmission of the vacuum windows, imperfect alignment of the retro-reflecting mirror, and beam clipping by the mirror, we did not completely reach 2π.

In reality, the attenuation and time delay of the second pulse affect the results of the experiment. Since the mirror was positioned $\sim$ 20 cm from the trap, there is a $\sim$ 680 ps time delay between the two pulses. This means that, given the 2.65 ns lifetime of the excited state, there is a significant chance ($\sim$ 23%) that the ion would decay between the first and second pulses, resulting in increased brightness at higher pulse energies, since near-π excitation by the first pulse results in about a $\sim$ 23% chance that the ion has decayed before the second pulse arrives, which then has the effect of moving the state population up again, instead of coherently moving the state population down from the upper state, which would occur if the ion does not decay between the two pulses. The second pulse was also attenuated to a significant degree by beam clipping on the retro-reflecting mirror, imperfect alignment of the retro-reflected pulse, and attenuation by the vacuum windows.

These two effects, attenuation and time delay, make direct calculation of the brightness probability very difficult. Therefore, we instead used a numerical simulation to estimate the bright state population as a function of pulse energy. This numerical solution utilized the optical Bloch equations (OBE), the parameters of the laser interaction, and the characteristics of the spontaneous decay of the excited state [30]. Using these equations, the brightness of the population was estimated as a function of laser pulse energy.

Once again, data were taken at a variety of different laser powers, with about $60,000$ runs per power setting. The data compared favorably with the estimations of the optical Bloch equations, showing similar general characteristics. The brightness as a function of laser power increases to a peak at about 1/6 bright when the initial pulse is a $\pi/2$ pulse. As pulse energy is increased beyond this level, the brightness decreases similarly to the OBE estimation. When the chance that the first pulse excites the ion is high, the effect of spontaneous emission increases the brightness. The comparison between the measured data and the numerically estimated state

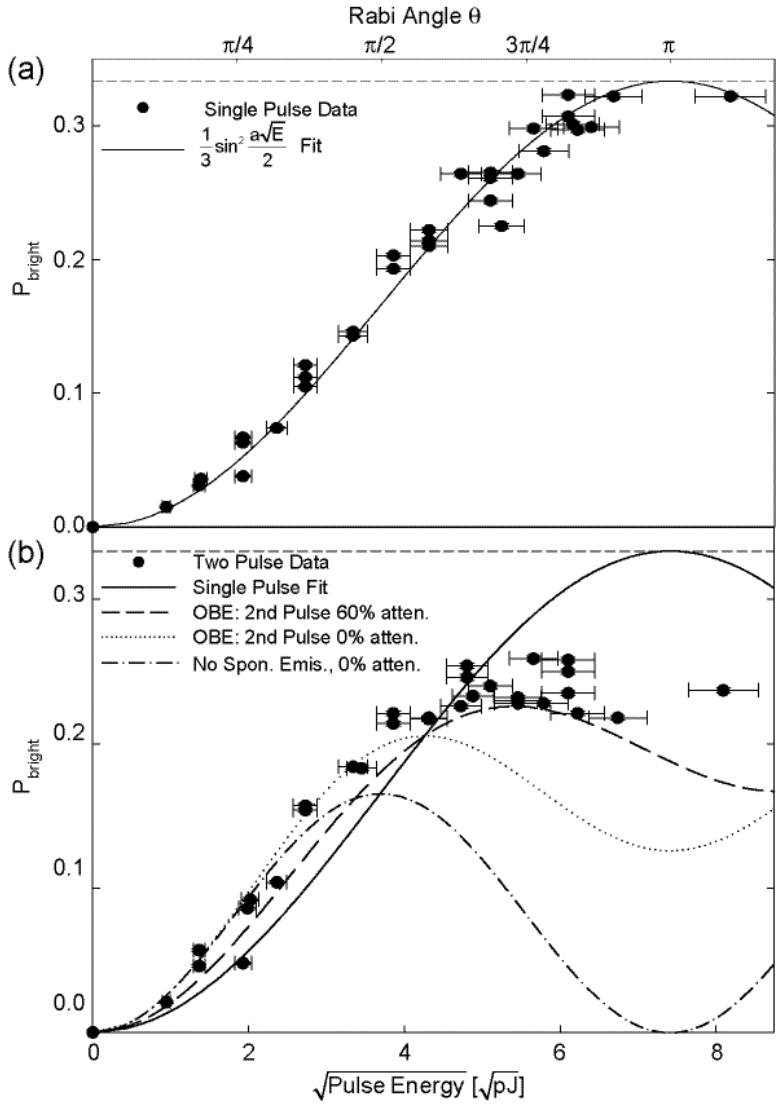

Figure 4.3: Data taken in the pulsed-laser Rabi experiment. (a) Graph for the ion brightness as a function of pulse energy for only one pulse. The probability of finding the ion in the bright state approaches 1/3 as laser pulse energy is increased as $1/3\sin^2(a\sqrt{P})$, as expected by theory. (b) Graph of ion brightness as a function of the energy in the first pulse, with a retroreflector in place to redirect the pulse onto the ion a second time. The brightness as a function of power is plotted against theory curves generated by using the optical Bloch equations (OBE). The theory predicts ion brightness will approach a maximum with about half as much power as is required with one pulse, and then turn downward when the second pulse's effect is to de-excite the ion. The experimental values have similar shape to the theory curves, with differences attributed to difficulties in characterizing the losses in retro-reflection of the light pulse. Shown are two theory curves for two different attenuations of the retro-reflected beam, which show how dramatically the results can change depending on the retro-reflection quality.

populations are shown in Fig. 4.3.

4.2 Pulsed Laser Ramsey Experiment

Once it was seen that ultrafast pulses in our system could coherently excite the ion from the S to P state, the next step was to place the same experiment into a Ramsey interferometer to measure how well a superposition of qubit states is maintained under ps excitation. The same ps laser pulses as before were now placed between two microwave pulses which rotate the population between the $\mid 0,0\rangle$ ($\mid \uparrow\rangle$, dark) and $\mid 1,0\rangle$ ($\mid \downarrow\rangle$, bright) states of the $S_{1/2}$ hyperfine structure. The microwave pulses used correspond to a rotation angle of $\pi/2$, resulting in a transfer from the prepared state, $\mid \uparrow\rangle$, to a 50-50 superposition of the two states, $(\mid \uparrow\rangle + \mid \downarrow\rangle)$.

The ion was then exposed to a ps pulse which transfers the population between the S and P states as before. Again, the ps pulse energy is determined by a variable attenuator and the light is π polarized. The transitions driven by the laser are limited to one for each state of the superposition, with $\mid \uparrow\rangle$ only driven to the $P_{3/2}|1,0\rangle$ state ($\mid \uparrow'\rangle$), and with $\mid \downarrow\rangle$ only driven to the $\mid 2,0\rangle$ state ($\mid \downarrow'\rangle$). It is notable that the bandwidth of our laser ($\sim$ 420 GHz) is ideal for this experiment: the $P_{1/2}$ and $P_{3/2}$ transitions are separated by 78000 GHz, which is much greater than the bandwidth of our laser and the transitions for the two S hyperfine states to the two P hyperfine states are separated by 13.9 GHz, which is much smaller than our laser bandwidth. Therefore, our laser is able to excite both transitions to the $P_{3/2}$ state without appreciably exciting the $P_{1/2}$ state. This selective excitation would be more difficult with a significantly faster or slower pulse, owing to increased or decreased bandwidth.

As previously discussed, the results of the Ramsey experiment without any intermediate perturbation is a simple $\cos^2$ curve with respect to the relative phase of the two pulses. Now, with ps excitations between the microwave excitations, we expect to see significant changes in the brightness as a function of phase. For the sake of simplicity, we define the contrast of the Ramsey fringes to be the amplitude of a corresponding fit to a $\cos^2$ function, such that the contrast ranges from zero (the brightness is not a function of phase) to one (the brightness is

fully determined by the phase). Decreasing contrast suggests that the coherence of the system was lost during the experiment.

In this experiment, the main source of coherence loss is linked to the spontaneous emission of photons during the experiment. When the ion is excited to the $P_{3/2}$ state, it spontaneously emits a photon whose frequency depends on the state of the qubit. Since the states of the qubit and photon frequency are entangled, measurement of the photon collapses the state of the qubit. In this experiment, the photons are measured by the environment, which leads to collapse of the qubit coherence.

When we apply only one ps pulse to the ion, we expect contrast to be $(1 - P_{\text{excit}})$. As before, we set the attenuator to a variety of levels, but this time we measured Ramsey contrast at each attenuation by measuring the brightness of the ion as a function of the phase of the second microwave pulse. The plot of brightness versus phase angle has the form

$$P_{\text{bright}} = v_{\text{off}} + A\cos^2(\theta/2 + \delta)$$

Here, θ is the phase angle of the second microwave pulse. δ is an overall phase angle caused by the delay between the two microwave pulses. v_{off} is an offset related to the probability of excitation to the P state; if the ion is excited to the P state with probability P_{exc}, we expect to see an increase in the overall brightness caused by the fact that spontaneous emission of $|\uparrow'\rangle$ has a 1/3 probability to end up in the bright state, and spontaneous emission of the $|\downarrow'\rangle$ cannot couple to the dark state ($\Delta F = 2$). Thus, v_{off} is equivalent to $(1/2)(1/3)P_{\text{exc}}$, since only half of the population is excited to the $|\uparrow'\rangle$ state when excitation occurs. A is the amplitude of the Ramsey fringes, and is also related to the probability of excitation: $A = (1 - P_{\text{exc}})$.

The data is compared to the expected curve for the contrast as a function of power calculated from the now-known probability of excitation as a function of laser power, and is found to be in good agreement with theory. As the laser power is varied, the contrast decreases almost completely to zero at the pulse energy corresponding to a π pulse. In addition, the individual curves of brightness as a function of phase angle and power match theory very closely.

As before, limited laser power resulted in a maximum Rabi angle of about π. Therefore, with one pulse, all that was observed was the extinction of Ramsey fringes as a function of power. In order to demonstrate coherence, we must show that the Ramsey fringes can be coherently recovered.

As before, we achieved additional excitation by retro-reflecting the pulse back onto the ion, resulting in addition of a second pulse attenuated by about 60% and delayed by ~ 680 ps from the first. The effect of the second pulse can be approximated by examining a simplified system. The first pulse excites the ion as before, rotating its state population toward the $P_{3/2}$ state. If we ignore spontaneous emission between the two pulses, the effect of the second pulse again varies according to the effect of the first. When the first pulse moves the state population about halfway between the S and P states, we expect that the effect of the second pulse will be washed out by the motion of the ion, as before. However, when the first pulse is approximately a π pulse, the relative optical phase becomes irrelevant and we expect the second pulse to move the population back down, restoring some contrast. The addition of spontaneous emission only hurts the contrast, resulting in incomplete contrast revival when both pulses are approximately π pulses.

Once again, the interactions of these pulses with the state of the ion is complicated and best solved numerically. Again using the optical Bloch equations, we numerically solved for the contrast as a function of laser pulse energy. Additionally, we solved the equations for several different attenuations of the second beam. The qualitative behavior of the solutions is gradual decrease of contrast to zero for a Rabi angle between $\pi/2$ and π (the exact location of the minimum depends on attenuation), followed by partial return of the contrast for larger Rabi angles, with a maximum contrast at π, where the first pulse excites completely and the second pulse coherently de-excites the ion.

Once again, we took data for a series of pulse energies, measuring contrast as a function of pulse energy. As we increased the pulse power, we indeed observed gradual decrease in the contrast to zero, followed by a return of the contrast. The plots of data versus numerical

solutions are shown in Fig. 4.4. The numerical estimates are reasonably close to the data.

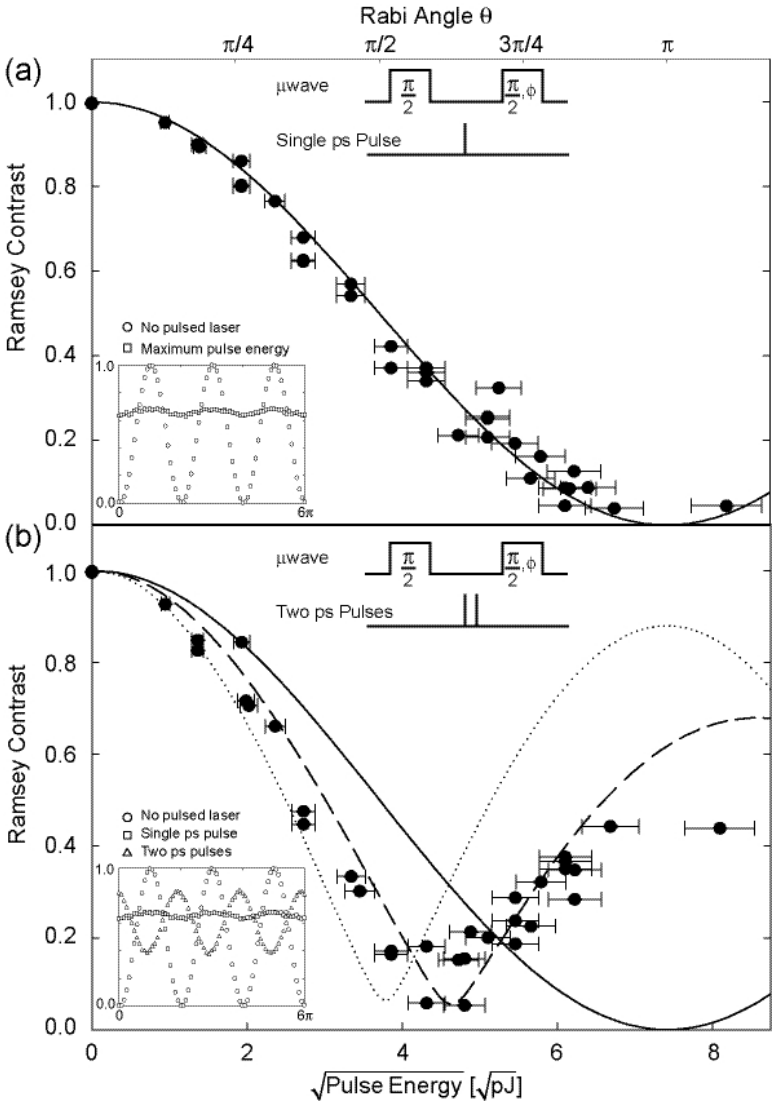

Figure 4.4: Data taken in the pulsed-laser Ramsey experiment. (a) First is shown the contrast as a function of applied laser pulse energy, which behaves in much the same way as the single-pulse Rabi experiment. The single pulse has excitation probability $P_{exc} = \cos^2(a\sqrt{P})$, where the same a as the Rabi experiment is used. If excitation occurs, spontaneous emission occurs before the second microwave pulse and all coherence is lost. (b) Once the second pulse is added, the dynamics of the system become more complicated. As in the two-pulse Rabi experiment, the second pulse causes the coherence to reach a minimum at about half the power of the one-pulse experiment, when the two pulses tend to cause spontaneous emission, and the coherence again reaches a maximum when the first pulse excites and the second de-excites, leaving the ion in the state it started. The curves are the predictions from the optical Bloch equations with the same second pulse attenuations as Fig. 4.3. From the inset, the phase shift seen when contrast was restored is clearly visible. The phase shift from the time spent in the excited state is clearly visible, and corresponds to a phase shift of about 18.9π.

An interesting point concerns the phase of the fringes as we increased the power. When we observed the return of the fringes, we noted that they were shifted by almost 180 degrees from each other. Careful consideration of the system suggests a good reason for this phase shift.

When we excite the ions from the $|\uparrow\rangle$ and $|\downarrow\rangle$ to the $|\uparrow'\rangle$ and $|\downarrow'\rangle$ levels, the frequency difference between the two states changes. In the S state, the hyperfine splitting is 14.5 GHz. In the P state, the hyperfine splitting is less, approximately 600 MHz. This means that, assuming the ion does **not** spontaneously emit, when me measure the Ramsey fringes, their phase is shifted by $\delta_{hf}\tau$, where δ_{hf} is the difference between the two frequency splittings and τ is the time spent in the P state. All of the experiments in which the first pulse fully excites to the P level but the ion does not spontaneously decay are phase-shifted by this amount. Therefore, we see a phase shift related to the time delay between the two pulses. We realized after seeing the phase shift that the time spent in the excited state affected the phase in this way. Had we set the mirror in a position giving zero phase shift, we might not have noticed this effect, and we might not have measured the excited state hyperfine splitting.

The fact that this phase does change allowed us to perform a precise measurement of the $P_{3/2}$ state hyperfine splitting. The phase shift is given by $\delta_{hf}2dc$, where d is the effective path length between the ion and the mirror, c is the speed of light, and δ_{hf} is the frequency difference between the two hyperfine splittings, $\omega_{hf,S} - \omega_{hf,P}$.

Since the phase shift is directly proportional to the effective path length, we changed the experiment slightly to allow variation of this parameter. Instead of a rigidly attached curved mirror to refocus the ps pulse onto the ion, we used a rigidly attached lens and a flat mirror on an adjustable mount to change the effective path length. We set the first pulse to approximately a π pulse, aligned the reflected pulse onto the ion, and measured Ramsey fringes while varying the position of the mirror. Each given run of experiments with a given mirror distance was fit to a $\cos^2$ function and the resulting phase of the Ramsey fringes was determined as a function of mirror distance. Using the above equation for the phase shift as a function of time between pulses, we fit a line to the phase data as a function of time delay between the two pulses. The

slope of this line is δ_{hf}, which, as stated above, is the difference between the two hyperfine splittings. Since the splitting of the $S_{1/2}$ level is well known, we were able to precisely determine the splitting of the $P_{3/2}$ level. Our final result for the splitting of the $P_{3/2}$ level is 626 ± 4 MHz.

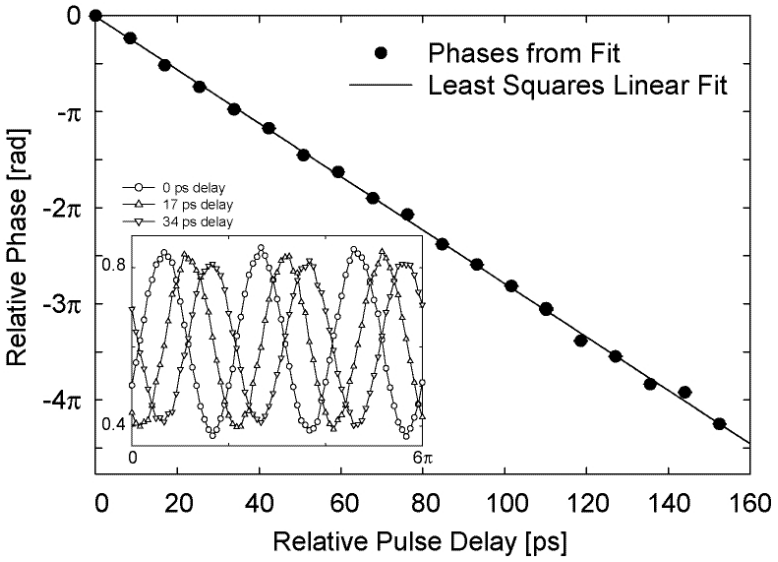

Figure 4.5: Data from moving the retro-reflecting mirror. Moving the mirror changes the time delay between the two pulses and thus changes their relative phase. The amount of phase change depends on the frequency difference between the hyperfine splittings in the S and P states, $\phi = (\omega_S - \omega_P)t$. The splitting of the S state is well known (≈ 14.5 GHz), so the hyperfine splitting of the P state can be determined from this data: $\partial\phi/\partial t = \omega_S - \omega_P$. The final result for the hyperfine splitting of the P state is $\omega_P = 626 \pm 4$ MHz.

Chapter 5

Conclusion

The experiments we performed showed that trapped ion systems can be excited with unit probability by ultrafast laser pulses. In addition, we showed that series of pulses can add coherently, cycling an ion's state population between two states without losing information stored in a quantum superposition. Coherent unit excitation is fundamental to the implementation of quantum gates that do not require cooling of ions to the ground motional state. This experiment shows that such excitations in a trapped ion system are experimentally achievable.

The particular shortcomings of this experiment were all technical in nature. For instance, the limited laser power is a result of the necessity of frequency-quadrupling, which severely limits the available power. Additionally, the retro-reflecting mirror limited the experiment by forcing attenuation of the second pulse and significant time delay between the pulses compared to the excited state lifetime. The primary source of error in the measurement of the $P_{3/2}$ hyperfine splitting was statistical. All of these errors are due to the peculiarities of our experimental apparatus and ion system, and all of them can potentially be eliminated. For instance, ion species which do not require frequency-quadrupled laser light would have much more abundant laser power. The retro-reflecting mirror could be replaced by a beam splitter and delay line before the ion, making the time delay between the two pulses potentially very short. In short, most of the problems stem from the fact that the S to P transition in $^{111}Cd^{+}$is in the deep ultraviolet. This causes a number of difficulties.

Despite these difficulties, however, near-unit excitation and coherence were observed.

These results are valuable demonstrations of the practicality of ultrafast quantum gates. Easily-achievable quantum gates would simplify efforts toward a large-scale quantum computer. Future experiments will make use of a different ion system, ytterbium, which may have more desireable characteristics for this type of experiment. As a result, we expect to be able to perform even more detailed experiments in the future.

Bibliography

[1] J. Drees and W. Paul, Z. Phys. **180**, 340 (1964).

[2] Robert S. Van Dyck, Jr. , Paul B. Schwinberg, Hans G. Dehmelt, Phys. Rev. Lett. **59**, 26 (1987).

[3] H. Häffner *et al.*, Nature **438**, 643 (2005).

[4] D. Leibfried *et al.*, Nature **438**, 639 (2005).

[5] C. Monroe, D. M. Meekhof, B. E. King, and D. J. Wineland, Science **272**, 1131 (1996).

[6] D. L. Moehring *et al.*, Phys. Rev. A **73**, 023413 (2006).

[7] Karen R. Jonscher and John R. Yates III, J. Biol. Chem. **272**, 1735 (1997).

[8] J. I. Cirac and P. Zoller, Phys. Rev. Lett. **74**, 4091 (1995).

[9] Peter W. Shor, SIAM J.Sci.Statist.Comput. **26**, (1997) 1484.

[10] L. K. Grover, Phys. Rev. Lett. **79**, 325 (1997).

[11] David P. DiVincenzo, quant-ph/0002077 (2000).

[12] D. Stick, W. K. Hensinger, S. Olmschenk, M. J. Madsen, K. Schwab, and C. Monroe, Nature Physics, **2**, 36 (2006).

[13] W. K. Hensinger, S. Olmschenk, D. Stick, D. Hucul, M. Yeo, M. Acton, L. Deslauriers, C. Monroe, and J. Rabchuk, App. Phys. Lett. **88**, 034101 (2006).

[14] P. J. Lee *et al.*, Optics Lett. **28**, 1582 (2003).

[15] C. Monroe, D. M. Meekhof, B. E. King, W. M. Itano, and D. J. Wineland, Phys. Rev. Lett. **75**, 4714 (1995).

[16] K. Mølmer and A. Sørensen, Phys. Ref. Lett. **82**, 1835 (1999).

[17] C. Simon and W. T. M. Irvine, Phys. Rev. Lett. **91**, 110405 (2003).

[18] L. -M. Duan, B. B. Blinov, D. L. Moehring, and C. Monroe, Quantum Inf. Comput. **4**, 165, (2004).

[19] L. -M. Duan and R. Raussendorf, Phys. Rev. Lett. **95**,080503 (2005).

[20] J. F. Poyatos, J. I. Cirac, R. Blatt, and P. Zoller, Phys. Rev. A **54**, 1532 (1996).

[21] J. J. Garcia-Ripoll, P. Zoller, and J. I. Cirac, Phys. Rev. Lett. **91**, 157901 (2003).

[22] S. -L. Zhu, C. Monroe, and L. -M. Duan, Europhys. Lett. **73**, 485 (2006).

[23] D. J. Wineland, C. Monroe, W. M. Itano, D. Leibfried, B. E. King, and D. M. Meekhof, J. Res. Natl. Inst. Stand. Technol. **103**, 259 (1998).

[24] D. Leibfried, R. Blatt, C. Monroe, D. Wineland, Rev. Mod. Phys. **75**, 281 (2003).

[25] D. J. Wineland and Wayne M. Itano, Phys. Rev. A **20**, 1521 (1979).

[26] L. Deslauriers, P. C. Haljan, P. J. Lee, K. -A. Brickman, B. B. Blinov, M. J. Madsen, and C. Monroe, Phys. Rev. A **70**, 043408 (2004).

[27] P. J. Lee *et al.*, J. of Optics B **7**, S371 (2005).

[28] David J. Griffiths, Introduction to Quantum Mechanics, second edition (Pearson Education, Inc., Upper Saddle River, NJ, 2005).

[29] W. W. Macalpine and R. O. Schildknecht, Proc. IRE **959**, 2099 (1959).

[30] Harold J. Metcalf and Peter van der Straten, Laser Cooling and Trapping (Springer-Verlag, New York, NY, 1999).